Master Thesis

Quasi-adiabatic preparation of squeezed antiferromagnetic states

Mar López I Iglesias

Supervisor: Dr. Darrick Chang
Co-supervisor: Dr. Błażej Jaworowski

Presentation date: 16 July 2026

Universitat de Barcelona
Master in Quantum Science and Technology Barcelona
ICFO

Quasi-adiabatic preparation of squeezed antiferromagnetic states

Mar López I Iglesias

Supervised by: Darrick Chang and Błażej Jaworowski

ICFO-Institut de Ciencies Fotoniques, The Barcelona Institute of Science and Technology, 08860 Castelldefels (Barcelona), Spain.

July 6, 2026

Cavity-mediated interactions have recently been proposed as a route toward strongly correlated many-body regimes in atomic ensembles. The underlying mechanism is that an antiferromagnetic cavity-mediated interaction penalises total transverse spin fluctuations, pushing the system toward states of small total spin, where the physics is determined by the cavity fluctuations. Once the system reaches a degenerate singlet-like sector, additional spatially structured spin couplings lift the degeneracy and select specific many-body phases, such as quantum spin liquids. This thesis addresses the first of these steps: the quasi-adiabatic preparation of squeezed antiferromagnetic states in a collective cavity-QED setting. We consider two atomic sublattices initialised in a classical antiferromagnetic product state pinned by a staggered field, and ramp up a cavity-mediated interaction that generates correlations between the sublattices, suppressing their collective transverse fluctuations. Since the cavity is intrinsically lossy, we describe the dynamics with a Lindblad master equation for collective photon loss, which introduces a competition between diabatic excitations from fast ramps and dissipative degradation from slow ones. We solve this trade-off in the minimal two-atom case, where the target is the antisymmetric Bell state, and then extend the analysis to larger ensembles using linear spin-wave theory, where the target is a two-mode squeezed antiferromagnetic state. In both regimes, the optimal protocol is not the most adiabatic one, but the one that best balances diabatic and dissipative errors. As the atom number increases, the achievable squeezing improves monotonically despite collective dissipation, approaching Heisenberg-limited scaling ($\propto 1/N$) in the weak-dissipation regime. These results show that squeezed antiferromagnetic states remain accessible under realistic cavity-QED conditions, supporting their role as a collective precursor toward richer, spatially structured many-body phases.

Keywords: Cavity quantum electrodynamics, quasi-adiabatic preparation, spin squeezing, collective dissipation.

Mar López I Iglesias: mlopezig59@alumnes.ub.edu

Acknowledgements

I would first like to thank my supervisors, Darrick Chang and Błażej Jaworowski, for their guidance throughout this project, for their patience with my questions, and for always pushing me to understand the physics behind the equations rather than just the equations themselves.

I am also grateful to the rest of the group: Charlie-Ray Mann and Mark Oehlgrien, whose earlier work laid the foundation on which this thesis builds, and my fellow master's student Albert Jiménez for the good company throughout the year.

To my master's friends, Ekaitz Martín, Lidija Petrovic, José Javier Fernández, and Blanca Belmonte, and to all my classmates: thank you for making this intense year such a good one, both in the classroom and outside of it.

Finally, to my family: my mother Mònica, my father Yuri, and my brother Bernat, thank you for your unconditional support. And to Martí, thank you for your patience and for your unconditional support through every high and low of this year. I could not have done this without any of you.

Contents

1 Introduction

Cavity quantum electrodynamics (QED) describes systems in which atoms are coupled through a common delocalised cavity mode, giving rise to effective collective interactions between many atoms [LSSV10, MPDR21, RDBE13]. By the collective nature of the interaction, these systems realise phenomena that can be described in terms of a single macroscopic spin, such as superradiant transitions [SBY+25] and collective spin squeezing [LSSV10, MNSZ19]. However, more recently, cavity-mediated interactions have also been proposed as a route towards strongly correlated many-body regimes, where this macroscopic-spin picture breaks down [MOJ+25]. The key idea is to use antiferromagnetic collective interactions that energetically favour states with a small total spin while penalising states that represent a macroscopic spin. The collective interactions therefore push the system into a highly entangled regime. For strong cavity-mediated interactions, the system is pushed to a singlet-like sector. The addition of perturbative short-range interactions then imprints a local structure into the entangled states, such that the system can realise exotic many-body spin phenomena, like quantum spin liquids [SB, BCK+20].

An important practical question is how to prepare such singlet-like states. This is nontrivial for two main reasons. First, the cavity-mediated interaction favours low total spin states rather than simply reinforcing classical antiferromagnetic order. As a result, the preparation requires building correlations between the two sublattices and tracking a state that is no longer well described by a simple symmetry-broken order parameter [MOJ+25]. Second, cavity-QED platforms are intrinsically open systems, so photons can leak out of the cavity, and atoms may also emit into free space [MPDR21, Cha24b]. A complete description of the preparation protocol would therefore have to treat many-body correlations, competing short-range and long-range interactions, and open-system dissipation on the same footing, which is extremely challenging.

A natural way to make this preparation problem more tractable is to separate it into two stages. The first stage uses the collective cavity interaction to build correlations in the antiferromagnet and prepare a squeezed antiferromagnetic precursor with reduced total transverse spin fluctuations. The second stage, not addressed in this thesis, would use spatially structured spin couplings to select a specific many-body phase within the resulting low-spin, singlet-like regime. In this thesis, we focus on the first stage of this strategy. The central objective is to determine the optimal two-mode squeezing that can be reached during the collective adiabatic stage and to establish how this optimum scales with the system size. To this end, we propose a quasi-adiabatic protocol. In an ideal closed system, this protocol is motivated by the adiabatic theorem: if a system is initialised in the ground state of a Hamiltonian and the Hamiltonian is changed sufficiently slowly, the state remains close to the instantaneous ground state [Ste19]. In a cavity-QED setting, however, the system is open, and photon leakage introduces collective dissipation during the same preparation process. The protocol must therefore be slow enough to suppress diabatic excitations, but fast enough to avoid excessive dissipative loss. We consider an effective spin Hamiltonian with two competing terms: a staggered field, which favours a classical antiferromagnetic product state, and a cavity-mediated interaction, which penalises total transverse spin fluctuations. The system is initialised in the classical antiferromagnetic product state pinned by the staggered field. The cavity-mediated interaction is then ramped up over time so that the state approximately follows the instantaneous ground state, developing correlations between the two sublattices that suppress total transverse spin fluctuations. We study this competition first in the two-atom case, where the target is the antisymmetric Bell state, and then for larger atom numbers using linear spin-wave theory, where the target is a two-mode squeezed antiferromagnetic state.

The main result of this work is that the optimal preparation is not simply the most adiabatic one. Instead, it is set by a balance between diabatic errors and collective photon loss. In the two-atom case, this balance determines the best Bell-state fidelity that can be reached. In the many-atom case, it determines the optimal two-mode squeezing and its dependence on system size. We find that collective dissipation reduces the achievable squeezing, but does not remove the improvement with atom number over the range studied. This shows that squeezed antiferromagnetic states can remain accessible in realistic cavity-QED settings, and supports their role as useful collective precursor states for later stages where spatial interactions may select more strongly correlated many-body phases.

The thesis is organised as follows. We begin by developing the effective model used throughout the work. This includes the cavity-mediated collective interaction, the staggered field that pins the initial antiferromagnetic state, and the quasi-adiabatic protocol used to ramp the cavity strength in the coherent limit. Collective dissipation is then introduced through a Lindblad master equation, which allows us to describe photon loss from the cavity during the preparation. We next turn to the two-atom case, which serves as a minimal benchmark for the quasi-adiabatic protocol. In this setting, the preparation quality is quantified by the Bell-state fidelity, allowing us to compare coherent evolution with the case where collective photon loss is included. We finally analyse larger atom numbers within linear spin-wave theory, where the relevant target is a two-mode squeezed antiferromagnetic state. In this regime, we study how the achievable squeezing depends on atom number, ramp speed, and dissipation strength, before summarising the main conclusions and discussing possible extensions.

2 Model

2.1 Atom - cavity mode interaction

We consider a standard cavity-QED setup, where a two-level atom interacts with a quantised electromagnetic field confined between two mirrors. When the atomic transition is close to one cavity resonance, the dynamics can be restricted to a single relevant mode. In this regime, the atom–light interaction is described by the Jaynes–Cummings model (JCM) [Cha24b].
The JCM describes the coherent exchange of excitations between a two-level atom and a single quantised cavity mode [JC63]. It is obtained within the rotating-wave approximation, where only the near-resonant atom-photon exchange processes are retained and dissipation is neglected. The resulting Hamiltonian is

$$H_{\mathrm{JCM}} = \frac{\hbar\omega_0}{2}\sigma^z + \hbar\omega a^\dagger a + \hbar g\left(\sigma^- a^\dagger + \sigma^+ a\right), \tag{1}$$

where ω_0 is the atomic transition frequency, ω is the cavity resonance frequency, σ^- and σ^+ are the atomic lowering and raising operators, a is the cavity-mode annihilation operator, and g is the atom-cavity coupling strength [Cha24b, Ste, SK93].

For an ensemble of identical two-level atoms coupled to the same cavity mode, the JCM generalises to the Tavis-Cummings model (TCM) [TC68]. In this case, the cavity mode couples to the collective spin operators

$$S^{\alpha} = \frac{1}{2}\sum_{j=1}^{N} \sigma_j^{\alpha}, \qquad S^{\pm} = \sum_{j=1}^{N} \sigma_j^{\pm}.$$

In the rotating frame of the atomic transition frequency, the atom-cavity dynamics is described by

$$H_{TCM} = \hbar\Delta_c a^{\dagger}a + \hbar g(aS^{+} + a^{\dagger}S^{-})\,,$$

where $\Delta_c = \omega - \omega_0$ is the detuning between the cavity mode and the atomic transition.

We now consider the dispersive regime, where the detuning is the largest energy scale of the system. In this limit, real exchange of excitations between the atoms and the cavity is strongly suppressed. The cavity therefore remains close to empty and photons are only virtually populated, meaning that they appear only as intermediate, short-lived excitations that mediate interactions between atoms [BGGW21]. This effective interaction can be obtained by completing the square

$$\frac{H_{\text{TCM}}}{\hbar} = \Delta_c \left(a^{\dagger} + \frac{g}{\Delta_c}S^{+}\right)\left(a + \frac{g}{\Delta_c}S^{-}\right) - \frac{g^2}{\Delta_c}S^{+}S^{-}\,.$$

The first term describes excitations of the displaced cavity mode. In the dispersive approximation, these excitations are projected out: the cavity field follows the atomic state adiabatically rather than being populated by real photons. Equivalently, the shifted mode $a + (g/\Delta_c)S^{-}$ is taken to remain in its vacuum. The remaining term gives the coherent effective interaction

$$H_{\text{eff}} = -\hbar\frac{g^2}{\Delta_c}S^{+}S^{-}.$$

Using $S^{\pm} = S^{x} \pm iS^{y}$,

$$S^{+}S^{-} = (S^{x})^2 + (S^{y})^2 + S^{z}.$$

The term proportional to S^{z} is a single-particle frequency shift and can be absorbed into the definition of the atomic transition frequency. Thus, the cavity-mediated collective interaction takes the form

$$H_{\text{cav}} = \lambda\left[(S^{x})^2 + (S^{y})^2\right]\,. \tag{2}$$

The resulting Hamiltonian characterises a collective infinite-range interaction mediated by virtual cavity photons whose strength is set by λ.

2.2 Physical system and Hamiltonian

The cavity-mediated interaction derived above couples only to the total collective spin of the ensemble. By itself, this collective term does not distinguish between the two sublattices or select any particular antiferromagnetic configuration. Since our goal is to study the collective squeezing of an antiferromagnetic state, we consider an ensemble divided into two sublattices, A and B, initially polarised in opposite directions. This provides the simplest collective description of a classical antiferromagnet and allows us to study how cavity-mediated interactions generate correlations between the two sublattices.

We therefore introduce collective spin operators S_{α}^{A} and S_{α}^{B} for the two sublattices. For N spin-1/2 atoms equally divided between A and B, each sublattice contains $N/2$ atoms and has a collective spin length $s = N/4$. To pin the initial antiferromagnetic configuration, we introduce a staggered longitudinal field that acts with opposite sign on the two sublattices. This can be interpreted as a Zeeman term in the Hamiltonian,

$$H_{\mathrm{Z}} = -\Delta \left(S_z^A - S_z^B \right), \tag{3}$$

where Δ denotes the strength of the staggered field. For $\Delta > 0$, this term favours spins in sublattice A pointing along $+\hat{z}$ and spins in sublattice B pointing along $-\hat{z}$, giving the classical antiferromagnetic product state.

Overall, the effective Hamiltonian studied in this work is

$$H(t) = \lambda \left((S_x^A + S_x^B)^2 + (S_y^A + S_y^B)^2 \right) - \Delta \left(S_z^A - S_z^B \right). \tag{4}$$

The first term describes the cavity-mediated interaction (2), written in terms of the total transverse spin of the two sublattices. The second term is the staggered field (3) that helps initialise the system as it favours the classical antiferromagnetic configuration.

The squeezing mechanism can be understood directly from the structure of the Hamiltonian (4), since the relative importance of the two terms is controlled by the parameters Δ and λ. When the longitudinal field dominates, the ground state is close to the classical AFM product state. This state has zero mean total magnetisation, $\langle S_\alpha^A + S_\alpha^B \rangle = 0$, but it still has transverse spin fluctuations. The relevant quantities are the variances of the total transverse spin components, $S_x^A + S_x^B$ and $S_y^A + S_y^B$. As the cavity strength λ is increased, the first term in the Hamiltonian assigns an energy cost to these total transverse fluctuations. The system can lower its energy by developing correlations between the two sublattices, so that their transverse fluctuations partially cancel in the total spin. In other words, a fluctuation of one sublattice in a transverse direction is accompanied by an opposite fluctuation of the other sublattice. The noise of the collective variables is therefore reduced, while the noise of the corresponding relative variables is increased. This redistribution of quantum noise is the two-mode spin-squeezing mechanism.

The Hamiltonian (4) suggests a possible path for squeezing. For fixed Δ, the nature of the ground state depends on the cavity strength λ. When $\lambda = 0$, the staggered field selects the classical antiferromagnetic product state. As λ is increased, the ground state lowers its energy by developing correlations between the two sublattices, becoming a squeezed antiferromagnetic state. Therefore, by making the cavity strength time-dependent,

$$\lambda \to \lambda(t)$$

the instantaneous ground state is continuously deformed from the classical antiferromagnetic product state into a squeezed antiferromagnetic state. This strategy is useful only if the actual quantum state can follow the changing ground state during the ramp, which brings us to the question of adiabaticity.

2.3 Adiabaticity and diabatic errors

The preparation protocol is based on the adiabatic theorem. In general, if a quantum system is initialised in the ground state of a Hamiltonian and the Hamiltonian is changed sufficiently slowly compared with the relevant energy gaps, the state remains close to the instantaneous ground state during the evolution [Ste19]. In our case, we use this idea to prepare the squeezed antiferromagnetic state. The system is initialised in the classical

AFM ground state for no cavity coupling, and the parameter $\lambda(t)$ is ramped over time. If the ramp is slow enough, the state follows the instantaneous ground state of (4) as it develops correlations between the two sublattices. If $\lambda(t)$ is changed too quickly, population is transferred to excited states, producing diabatic errors.

The goal is therefore to choose a ramp $\lambda(t)$ that changes the Hamiltonian slowly enough for the state to remain close to the instantaneous ground state, while still reaching the squeezed regime in a finite time. To formulate this requirement, we introduce the instantaneous eigenstates of the time-dependent Hamiltonian,

$$H(t)\,|n(t)\rangle = E_n(t)\,|n(t)\rangle\,,$$

where $|0(t)\rangle$ denotes the instantaneous ground state and $|n(t)\rangle$, with $n > 0$, denotes an instantaneous excited state. We quantify the degree of adiabaticity through the dimensionless parameter

$$\epsilon_n(t) = \left| \frac{\langle n(t)|\,\partial_t 0(t)\rangle}{E_n(t) - E_0(t)} \right|. \tag{5}$$

The numerator measures how strongly the time dependence of the Hamiltonian couples the instantaneous ground state to the excited state $|n(t)\rangle$, while the denominator is the corresponding energy gap. The adiabatic condition requires $\epsilon_n(t) \ll 1$ for all relevant excited states throughout the ramp. The smaller this ratio is throughout the ramp, the closer the evolution remains to the adiabatic limit. When this condition is not satisfied, population can be transferred out of the instantaneous ground state, producing diabatic errors.

The adiabatic parameter provides a practical way to choose the ramp speed. Instead of varying $\lambda(t)$ linearly in time, we can adapt the speed of the ramp to the instantaneous spectrum of the Hamiltonian. The idea is to move slowly in regions where the ground state is more sensitive to changes in λ, or where the energy gap to excited states is small, and faster where the evolution is naturally more adiabatic. This is done by fixing the adiabatic parameter to a constant value, $\epsilon(t) = \epsilon_0$, which defines a locally optimised ramp. The value of ϵ_0 controls the total ramp duration: smaller ϵ_0 correspond to slower and more adiabatic protocols, while larger ϵ_0 yield faster ramps with stronger diabatic errors.

In a closed system, one would therefore expect the preparation to improve monotonically as ϵ_0 is reduced. However, in a realistic cavity-QED implementation, the coherent interaction is not the only process present. The same cavity mode that mediates the effective spin interaction can also lose photons to the environment, producing a collective dissipative channel. This introduces a competing error mechanism: making the ramp slower suppresses diabatic excitations but also gives dissipation more time to degrade the state. The optimal preparation is therefore determined by a balance between these two effects, which motivates the inclusion of collective dissipation in the following section.

2.4 Collective dissipation

To describe the second source of error in the preparation protocol, we now include the effect of collective dissipation. This term represents the loss channel associated with the cavity mode itself. Photons can leak through the cavity mirrors into the external environment. Since all atoms couple to the same cavity mode, this loss process acts on the ensemble collectively rather than on each atom independently. If the emitted light is not monitored, the information carried away by these photons is lost, and the atomic state can no longer be described by purely unitary evolution; rather, it must be described by a density matrix.

In this work, we model this process as Markovian. This means that the emitted photons do not return to interact with the atoms again, so the environment does not retain memory that affects the later dynamics of the system. Under this assumption, the evolution is described by a Lindblad master equation,

$$\begin{aligned} \dot{\rho}(t) &= -\mathrm{i}[H(t), \rho(t)] + \mathcal{D}_L[\rho(t)] \,, \\ \mathcal{D}_L[\rho(t)] &= \Gamma(t) \left(L\rho(t)L^\dagger - \frac{1}{2}\{L^\dagger L, \rho(t)\} \right) \,, \\ \Gamma(t) &= \eta\lambda(t) \,. \end{aligned} \tag{6}$$

Here, the first term describes the coherent evolution generated by the Hamiltonian (4), while the second term is the dissipator associated with collective photon loss. This channel is described by the collective jump operator $L = S_-^A + S_-^B$, which acts on the two sublattices as a whole rather than representing independent decay processes for each atom. Since both the coherent interaction and the collective dissipation originate from the same atom-cavity coupling, we take the dissipation rate to have the same time dependence as the cavity-mediated interaction, $\Gamma(t) = \eta\lambda(t)$. The dimensionless parameter η controls the relative strength of dissipation compared with the coherent dynamics, and depends on microscopic parameters such as the cavity linewidth and microscopic detunings.

With both the diabatic excitations and dissipative losses, the protocol is directly affected by the competing error mechanisms. If the ramp is too fast, diabatic excitations prevent the state from following the instantaneous ground state. But if it is too slow, the system spends more time exposed to dissipative processes. Consequently, the optimal protocol is expected to occur at an intermediate stopping time, where the benefits of improved adiabaticity are balanced by the accumulated dissipative noise.

3 The two-atom case

The simplest case of the collective antiferromagnetic model is obtained by considering only two atoms, $N = 2$. In this limit, the system is small enough to obtain analytical results and provides a transparent setting in which to understand the basic mechanism of the protocol. The two-atom problem should therefore be viewed as a minimal test case for the preparation protocol. It contains the same basic ingredients as the many-body problem and, at the same time, the Hilbert space is small enough that the dynamics and the target singlet can be understood analytically. In this small setting, the target state is the antisymmetric Bell state

$$|S\rangle = \frac{|\uparrow\downarrow\rangle - |\downarrow\uparrow\rangle}{\sqrt{2}} \,. \tag{7}$$

Then, the most direct way of measuring the success of the protocol is the Bell state fidelity; in other words, the overlap between the found state and the singlet (7). For a mixed state, the fidelity with a pure state is given by the expectation value of the corresponding projector,

$$F_{\mathrm{Bell}}(t) = \mathrm{Tr}[|S\rangle\langle S|\, \rho(t)] = \langle S|\, \rho(t)\, |S\rangle \,. \tag{8}$$

For two atoms, the full Hilbert space is four-dimensional, with basis $\{|\uparrow\uparrow\rangle, |\uparrow\downarrow\rangle, |\downarrow\uparrow\rangle, |\downarrow\downarrow\rangle\}$. However, the Hamiltonian (4) conserves the total magnetisation $M = S_z^A + S_z^B$. Since the protocol starts from the antiferromagnetic state $|\uparrow\downarrow\rangle$, which belongs to the $M = 0$

sector, the coherent dynamics remains within the subspace spanned by $\{|\uparrow\downarrow\rangle, |\downarrow\uparrow\rangle\}$. The states $|\uparrow\uparrow\rangle$ and $|\downarrow\downarrow\rangle$ belong to the sectors $M = +1$ and $M = -1$, respectively, and are not coupled to the antiferromagnetic sector by the Hamiltonian. In this $M = 0$ subspace, the Hamiltonian (4) takes the form

$$H(t) = \begin{pmatrix} \lambda(t) - \Delta & \lambda(t) \\ \lambda(t) & \lambda(t) + \Delta \end{pmatrix},$$

as found in the Appendix A.1. By diagonalizing this matrix, we can obtain the analytical expression for the eigenenergies

$$E_\pm = \lambda(t) \pm \sqrt{\Delta^2 + \lambda(t)^2}$$

and for the ground state

$$|g(t)\rangle = \cos\frac{\theta(t)}{2}\,|\uparrow\downarrow\rangle - \sin\frac{\theta(t)}{2}\,|\downarrow\uparrow\rangle \quad \text{where} \quad \tan\theta(t) = \frac{\lambda(t)}{\Delta(t)}\,.$$

This instantaneous ground state is the relevant state because the preparation protocol is based on adiabatic following. In the ideal adiabatic limit, the physical state would remain equal to $|g(t)\rangle$ throughout the ramp. The overlap between the ground state of the coherent Hamiltonian and the Bell state (7) gives the ideal coherent Bell fidelity,

$$F_{\text{Bell}}(t) = \langle S|\,g(t)\rangle\,\langle g(t)|\,S\rangle = \frac{1}{2}\Big[1 + \sin\theta(t)\Big] = \frac{1}{2}\Big[1 + \frac{\lambda(t)}{\sqrt{\Delta^2 + \lambda(t)^2}}\Big]\,.$$

This expression gives the ideal adiabatic Bell fidelity without taking into account any diabatic errors or dissipative losses. It gives the fidelity that would be obtained if the state followed the instantaneous ground state perfectly during the ramp. It depends only on the ratio $\Delta/\lambda(t)$ and it reaches its maximum value for $\Delta/\lambda(t) \to 0$.

In practice, the ramp has to be performed in a finite time. The state cannot follow the instantaneous ground state perfectly, and part of the population can be transferred to the instantaneous excited state.
To reduce these errors in a controlled way, we use the adiabatic parameter introduced in Eq. (5) to design the ramp. We choose $\lambda(t)$ by imposing a constant value $\epsilon(t) = \epsilon_0$. This makes the ramp slower in the regions where the instantaneous ground state is more strongly coupled to the excited state or where the energy gap is smaller, and faster where the evolution is naturally more adiabatic. In this sense, the protocol ensures that the evolution remains equally adiabatic along the ramp. The analytical form of this optimised ramp is

$$\lambda(t) = \frac{4\epsilon_0\Delta^2 t}{\sqrt{1 - (4\epsilon_0\Delta t)^2}}\,, \tag{9}$$

and its derivation is given in the Appendix A.2.

If photon leakage from the cavity is also included, the two-atom system must be described using the Lindblad master equation introduced in Eq. (6). In this case, the collective jump operator $L = S_-^A + S_-^B$ does not preserve the $S_z = 0$ subspace, so the system should be described in the enlarged basis $\{|\uparrow\downarrow\rangle, |\downarrow\uparrow\rangle, |\downarrow\downarrow\rangle\}$, where the density matrix takes the form

$$\rho(t) = \begin{pmatrix} p_a(t) & x(t) + iy(t) & 0 \\ x(t) - iy(t) & p_b(t) & 0 \\ 0 & 0 & p_c(t) \end{pmatrix}.$$

With this parametrisation, $p_a(t)$ and $p_b(t)$ are the populations of the two antiferromagnetic states, $|\uparrow\downarrow\rangle$ and $|\downarrow\uparrow\rangle$ respectively. The off-diagonal element $x(t) + iy(t)$ gives their coherence, which distinguishes a quantum superposition from a classical mixture. Lastly, $p_c(t)$ is the population transferred to $|\downarrow\downarrow\rangle$ by collective dissipation.

Following the strategy detailed in Appendix A.3, the Lindblad master equation reduces to the following closed set of real differential equations:

$$\begin{aligned}
\dot{p}_a(t) &= -2\lambda(t)y(t) - \Gamma(t)\left[p_a(t) + x(t)\right] , \\
\dot{p}_b(t) &= 2\lambda(t)y(t) - \Gamma(t)\left[p_b(t) + x(t)\right] , \\
\dot{p}_c(t) &= \Gamma(t)\left[p_a(t) + p_b(t) + 2x(t)\right] , \\
\dot{x}(t) &= -2\Delta y(t) - \Gamma(t)x(t) - \frac{\Gamma(t)}{2}\left[p_a(t) + p_b(t)\right] , \\
\dot{y}(t) &= 2\Delta x(t) - \lambda(t)\left[p_b(t) - p_a(t)\right] - \Gamma(t)y(t) .
\end{aligned} \tag{10}$$

The structure of these equations separates the coherent dynamics, governed by $\lambda(t)$ and Δ, from the collective dissipation dynamics, governed by $\Gamma(t)$. The population transferred to $|\downarrow\downarrow\rangle$ depends not only on $p_a(t)$ and $p_b(t)$, but also on the coherence $x(t)$, which reflects the collective nature of the dissipation. In particular, for the singlet state, one has $p_a = p_b = 1/2$ and $x = -1/2$, so $\dot{p}_c(t)$ vanishes, showing that (7) is a dark-state of the collective dissipation channel (it cannot emit collectively).

This real formulation is convenient for numerical integration. Instead of integrating the full complex density matrix directly, we integrate the real vector $\mathbf{r}(t) = (p_a(t), p_b(t), p_c(t), x(t), y(t))$ from the initial AFM product state $\mathbf{r}(0) = (1, 0, 0, 0, 0)$.

The Bell-state fidelity is obtained analytically by projecting the density matrix onto the singlet state (8):

$$F_{\mathrm{Bell}}(t) = \frac{1}{2}[p_a(t) + p_b(t) - 2x(t)] . \tag{11}$$

This expression shows that a high Bell fidelity requires the state to remain in the antiferromagnetic subspace while developing the correct relative phase between its two components. Population outside this subspace, such as population in $|\downarrow\downarrow\rangle$, does not contribute to the singlet overlap. Moreover, since $p_a(t) + p_b(t) \leq 1$, the population contribution alone is bounded by $1/2$. A Bell fidelity above this value is only possible if the coherence $x(t)$ is negative, as required by the relative minus sign between $|\uparrow\downarrow\rangle$ and $|\downarrow\uparrow\rangle$ in the singlet. In the ideal case, $p_a = p_b = 1/2$ and $x = -1/2$, giving $F_{\mathrm{Bell}} = 1$.

3.1 Results and discussion

We first study the preparation of the two-atom singlet in the absence of dissipation. We characterise the performance of the protocol through the Bell-state fidelity (11), calculated by numerically integrating the equations (10) for $\Gamma(t) = 0$, that is $\eta = 0$.

In the adiabatic limit, the system is expected to follow the instantaneous ground state. Therefore, the parameter ϵ_0 controls the trade-off between adiabaticity and evolution time: smaller values of ϵ_0 correspond to slower ramps and should lead to higher fidelities, whereas larger values produce faster but less adiabatic dynamics. The figures below show this dependence.

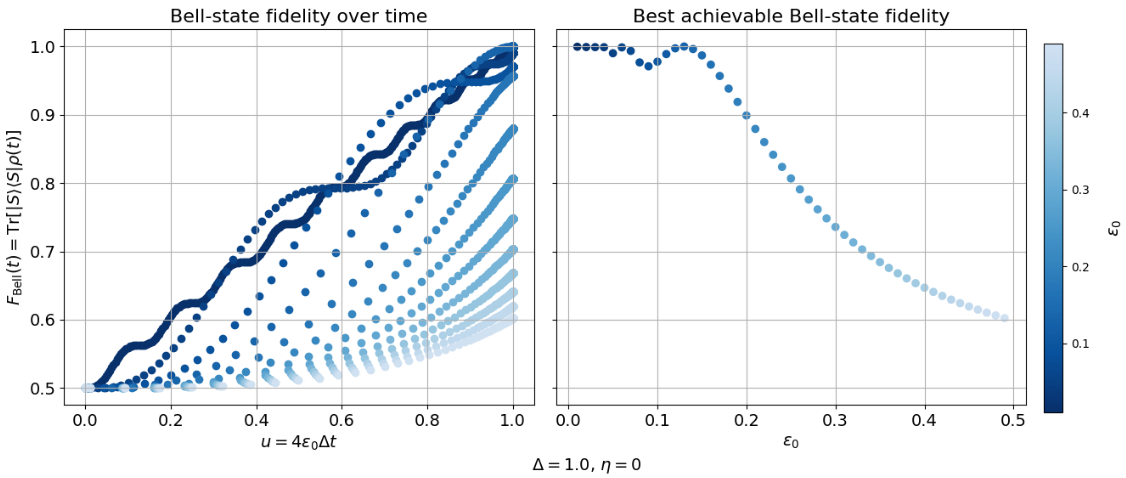

Figure 1: Coherent preparation of the two-atom singlet for $\Delta = 1.0$ and $\eta = 0.0$. The left panel shows the Bell-state fidelity (8) during the ramp as a function of the dimensionless time ($u = 4\epsilon_0\Delta t$) for different values of the adiabatic parameter, indicated by colour. The right panel shows the maximum Bell-state fidelity reached during the ramp as a function of ϵ_0.

The behaviour shown in Fig. 1 confirms the expected role of the adiabatic parameter. For the smallest values of ϵ_0, the Bell-state fidelity reaches values very close to unity, showing that the two-atom singlet can be prepared with high accuracy in the coherent limit. As ϵ_0 increases, the maximum fidelity decreases, indicating the increasing relevance of diabatic transitions.

In addition, for sufficiently small ϵ_0, small oscillations can be observed in the fidelity during the ramp. These oscillations are not captured by the ideal adiabatic prediction (3) since they originate from coherent interference between the instantaneous eigenstates. During a finite-time ramp, the evolved state is not exactly the instantaneous ground state, but also contains a contribution from the instantaneous excited state. Since these two components have different energies, they accumulate phase at different rates. This relative phase produces oscillations in the coherence $x(t)$ and, consequently, in the Bell-state fidelity. They are only visible for smaller values of ϵ_0 because the ramp is slow enough that the system has more physical time to undergo these coherent oscillations.

Having established the coherent reference case, we now include collective dissipation. In this case, making the ramp slower is no longer always beneficial. A smaller ϵ_0 makes the ramp more adiabatic and suppresses diabatic excitations, but it also increases the time over which dissipative effects can accumulate. The final fidelity is therefore determined by the competition between two error mechanisms: diabatic errors, which are more relevant for fast ramps, and dissipative losses, which become more important when the evolution lasts too long.

For this reason, the optimisation involves two independent choices. The parameter ϵ_0 fixes the speed of the locally optimised ramp, while the stopping time determines the point along the ramp at which the state is taken as the final prepared state. For each value of ϵ_0, the fidelity may reach a maximum at an intermediate time, before dissipation has had time to degrade the state significantly. We therefore optimise the Bell-state fidelity both over the ramp parameter ϵ_0 and over the stopping time. To study this competition, we use the same locally optimised ramp (9) and integrate the equations of motion (10) with a finite dissipation strength η. The results are showed in Fig. 2.

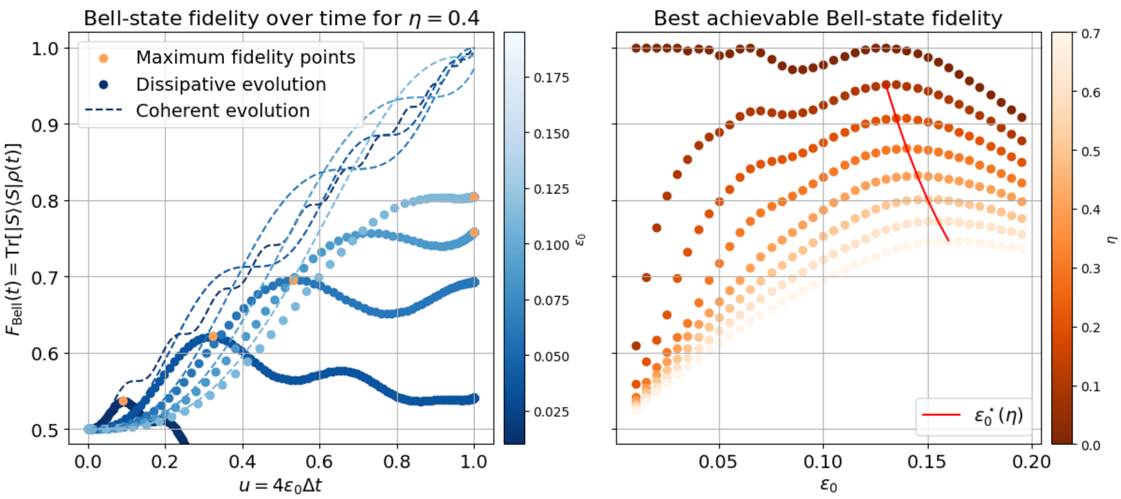

Figure 2: Effect of collective dissipation on the two-atom Bell-state preparation for $\Delta = 1.0$. The left panel shows the Bell-state fidelity (8) during the ramp as a function of the dimensionless time ($u = 4\epsilon_0\Delta t$) for $\eta = 0.4$ and different values of the adiabatic parameter, indicated by colour. The dashed curves correspond to the coherent reference case, while the solid curves show the evolution in the presence of collective dissipation. The orange markers indicate the maximum fidelity reached along each dissipative trajectory. These maximum values are then plotted in the right panel as a function of ϵ_0 for different dissipation strengths η, indicated by colour. For each value of η, the red line connects the value of ϵ_0 that gives the highest Bell-state fidelity, defining the optimal ramp parameter $\epsilon_0^*(\eta)$.

Figure 2 shows the effect of collective dissipation on the system's evolution over the ramp. In the left panel, the dissipative trajectories reach lower maximum fidelities than their coherent counterparts. For some ramps, the maximum fidelity is reached before the end of the protocol: after this point, continuing the evolution only allows dissipation to further degrade the state. The right panel makes the trade-off between diabatic and dissipative errors explicit and identifies the optimal value of the adiabatic parameter for each dissipation strength. For large values of ϵ_0, ramps are fast, and diabatic excitations evade the instantaneous ground state, reducing the fidelity. For small values of ϵ_0, longer evolution leads to the accumulation of dissipation, which also reduces the fidelity. Consequently, for each value of dissipation strength η, there is an optimal value of the adiabatic parameter ϵ_0^* that, at the same time, defines an optimal ramp speed. The relation between these parameters is visible in Fig. 3.

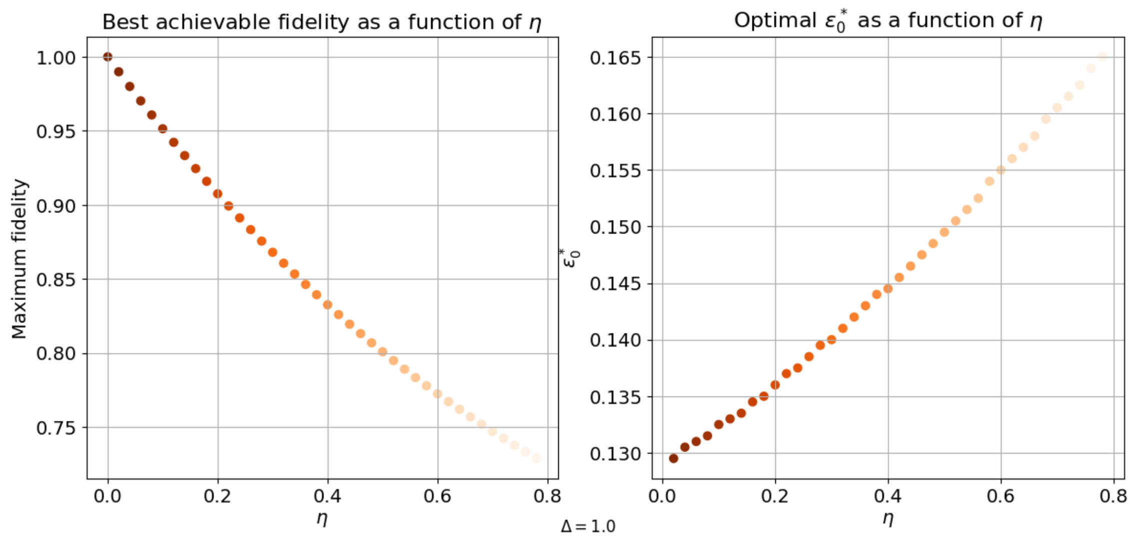

Figure 3: Dependence of the optimized two-atom Bell-state preparation on the collective dissipation strength η, for $\Delta = 1.0$. The left panel shows the best achievable Bell-state fidelity after optimizing over ϵ_0. The right panel shows the corresponding optimal ramp parameter $\epsilon_0^\star(\eta)$, which increases with η.

Figure 3 summarises the optimal performance of the dissipative two-atom protocol. The left panel shows that the best achievable Bell-state fidelity decreases as the dissipation strength η is increased. This confirms that collective losses limit the preparation quality. Even though the target singlet itself is a dark state of the jump operator $L\,|S\rangle = 0$, the system is not in the singlet state during the ramp, so it remains partially sensitive to the dissipative channel. The right panel shows the value of the adiabatic parameter that maximises the fidelity for each η. The optimal value $\epsilon_0^\star$ increases with the dissipation strength, meaning that stronger dissipation favours faster ramps. This is consistent with the trade-off discussed above: when losses are weak, the protocol can be slower and more adiabatic, whereas for larger η it becomes advantageous to reduce the evolution time, even at the cost of allowing more diabatic error. The optimal protocol is therefore obtained by balancing diabatic errors with the collective losses.

The study of the two-atom case has provided a minimal setting in which the main mechanisms of the protocol can be identified explicitly. In the coherent limit, the optimised ramp prepares the Bell singlet by suppressing diabatic transitions, while in the open-system setting, the achievable fidelity is limited by the competition between adiabaticity and collective dissipation. We now consider larger atom numbers, where the target is no longer a two-particle Bell state but a squeezed antiferromagnetic state involving collective quantum correlations between the two sublattices.

4 The N-atom case

Now we will consider larger system sizes. The objective is to determine how the optimal two-mode squeezing in the collective adiabatic stage scales with atom number N. In this case, the target state is no longer characterised by the Bell-state fidelity. Instead, we quantify the success of the protocol through the squeezing parameter

$$\xi^2 = \frac{N}{2} \frac{\langle S_x^2 + S_y^2 \rangle}{|\langle S_z^A \rangle - \langle S_z^B \rangle|^2}\,, \tag{12}$$

where $S_x = S_x^A + S_x^B$ and $S_y = S_y^A + S_y^B$ are the total transverse spin components. This quantity compares the transverse collective spin fluctuations with the remaining antiferromagnetic order. The numerator measures the residual fluctuations of the total transverse spin, which are precisely the fluctuations penalised by the cavity-mediated interaction. The denominator is proportional to the square of the staggered magnetisation, $|\langle S_z^A \rangle - \langle S_z^B \rangle|$, and therefore measures how strongly the two sublattices remain polarised in opposite directions. The prefactor $N/2$ is chosen so that the classical antiferromagnetic product state has $\xi^2 = 1$. Indeed, for the state with all spins in sublattice A pointing along $+\hat{z}$ and all spins in sublattice B pointing along $-\hat{z}$, one has $\langle S_z^A \rangle = N/4$ and $\langle S_z^B \rangle = -N/4$, so $|\langle S_z^A \rangle - \langle S_z^B \rangle|^2 = N^2/4$. At the same time, the transverse fluctuations are those of N independent spin-1/2 particles, giving $\langle S_x^2 + S_y^2 \rangle = N/2$. Substituting these values into Eq. (12) gives $\xi^2 = 1$. Values $\xi^2 < 1$ therefore indicate that the state has reduced collective transverse fluctuations compared with the classical AFM reference state, while still retaining antiferromagnetic order.

For large N, an exact treatment of the dynamics quickly becomes impractical for extracting asymptotic scaling. Even within the collective spin sector of the two sublattices, the Hilbert space grows with system size, and solving the full master equation becomes increasingly costly. We use linear spin-wave theory (LSWT) as the main analytical and numerical framework, as it provides direct analytical insight and remains efficient enough to study large systems.

4.1 Linear Spin-Wave Theory

To study the N-atom case, we use the Holstein-Primakoff (HP) transformation. The idea is to expand the spin dynamics around the classical antiferromagnetic product state. Instead of describing each individual spin, we describe small collective deviations from this classical configuration. These deviations are represented by bosonic modes. For sublattice A, the reference state is the fully polarised state along $+\hat{z}$. This state has maximal eigenvalue of S_z^A, namely $m_A = s$, and is identified with the bosonic vacuum. Adding one HP boson reduces this eigenvalue by one unit. More generally, a state with $n_a = a^\dagger a$ bosons corresponds to an eigenvalue $m_A = s - n_a$. For sublattice B, the reference spin points in the opposite direction, so the signs are reversed. The bosonic vacuum corresponds to $m_B = -s$, and a state with $n_b = b^\dagger b$ bosons has $m_B = -s + n_b$. In both sublattices, the boson number counts deviations from the local classical spin direction.

Using this transformation in each sublattice we can obtain the relations

$$\begin{aligned} S_z^A &= s - a^\dagger a, \quad S_+^A = \sqrt{2s - a^\dagger a}\, a, \quad S_-^A = a^\dagger \sqrt{2s - a^\dagger a}, \\ S_z^B &= b^\dagger b - s, \quad S_+^B = b^\dagger \sqrt{2s - b^\dagger b}, \quad S_-^B = \sqrt{2s - b^\dagger b}\, b. \end{aligned} \tag{13}$$

Here, $a^\dagger$ and $b^\dagger$ create symmetric spin-wave excitations on sublattices A and B relative to the classical AFM state, which is identified with the bosonic vacuum $|0\rangle_A |0\rangle_B$. For a system of N spin-1/2 atoms divided equally into two sublattices, each sublattice contains $N/2$ atoms. Since the spins within each sublattice are treated collectively, the maximum spin length of each sublattice is $s = N/4$. This is the spin length around which we perform the Holstein-Primakoff expansion.

While this mapping is formally exact, the LSWT consists of expanding the square roots in (13) around the classical AFM state and keeping only the leading terms in the bosonic operators [Cha24a]. This gives the linear spin-wave operators

$$\begin{aligned} S_z^A &= s - a^\dagger a, \quad S_+^A = \sqrt{2s}\, a, \quad S_-^A = a^\dagger \sqrt{2s}, \\ S_z^B &= b^\dagger b - s, \quad S_+^B = b^\dagger \sqrt{2s}, \quad S_-^B = \sqrt{2s}\, b. \end{aligned} \tag{14}$$

This approximation neglects interactions between spin waves and therefore remains controlled as long as the spin-wave density is small compared with the sublattice spin length,

$$\langle a^\dagger a \rangle, \ \langle b^\dagger b \rangle \ll 2s = \frac{N}{2}\,.$$

Physically, this means that the dynamics remains close to the classical AFM reference state and only a small fraction of the available spin length is converted into quantum fluctuations.

In the Hamiltonian (4), using the LSWT operators is equivalent to retaining terms up to quadratic order in the bosonic operators. This analysis, detailed in Appendix B.1, yields the LSWT Hamiltonian

$$\begin{gathered} H(t) = E_0(t) + A(t)(a^\dagger a + b^\dagger b) + B(t)(ab + a^\dagger b^\dagger), \\ \text{where } A(t) \equiv \Delta + \frac{N\lambda(t)}{2} \text{ and } B(t) \equiv \frac{N\lambda(t)}{2}. \end{gathered} \tag{15}$$

Here, $E_0(t) = N(\lambda(t) - \Delta)/2$ is a time-dependent energy offset proportional to the identity. It comes from the classical AFM reference energy and the part of the cavity term free of operators. Since it does not affect the equations of motion, it will be omitted in what follows.

The term in the LWST Hamiltonian (15) that is proportional to $A(t)$ gives the energy cost of creating spin-wave excitations on either sublattice. The next term, proportional to $B(t)$, does not conserve the number of spin waves: it creates or annihilates pairs of excitations, one in each sublattice. This is the key term responsible for generating correlations between the two sublattices. When $\lambda(0) = 0$, one has $B(0) = 0$ and the bosonic vacuum corresponds to the classical AFM state. As the cavity strength is increased, the term $a^\dagger b^\dagger$ creates pairs of spin-wave excitations, one in each sublattice, while the Hermitian-conjugate term ab annihilates such pairs. The instantaneous ground state is therefore no longer the simple AFM vacuum, but a superposition of states with correlated spin-wave excitations in the two sublattices. This is the squeezed antiferromagnetic state described within LSWT.

Following the procedure explained in the Model section 2.3, the Hamiltonian can be diagonalized in the instantaneous Bogoliubov basis to obtain an analytical expression for the adiabatic parameter introduced in Eq. (5). Although the general definition contains an index n, within LSWT the instantaneous ground state is a two-mode squeezed vacuum whose time dependence enters only through the squeezing parameter $\theta(t)$. As a result, $\partial_t \left|\theta(t)\right\rangle$ couples the ground state only to the Bogoliubov-pair excitation $\alpha^\dagger(t)\beta^\dagger(t)\left|\theta(t)\right\rangle$, so the relevant adiabatic parameter reduces to a single quantity, denoted by $\epsilon(t)$. Imposing $\epsilon(t) = \epsilon_0$ and solving for the cavity strength $\lambda(t)$ gives the locally optimised ramp

$$\lambda(t) = \frac{\Delta}{N}\left[(1 - 4\epsilon_0 \Delta t)^{-2} - 1\right]. \tag{16}$$

The derivation of this expression is given in Appendix B.2. This expression also makes clear that ϵ_0 controls the speed of the ramp. A smaller value of ϵ_0 enforces a more adiabatic evolution, so the same change in $\lambda(t)$ is performed more slowly. A larger value of ϵ_0 allows the ramp to move faster, but produces stronger diabatic errors. The total preparation time is determined not only by ϵ_0, but also by where the ramp is stopped. This distinction becomes important in the dissipative case, where the final squeezing depends both on how adiabatically the state is prepared and on how long dissipative effects have time to accumulate.

The LSWT Hamiltonian (15) is quadratic in the bosonic operators and therefore preserves Gaußian states under time evolution. Moreover, the collective jump operator $L = S_-^A + S_-^B$ that describes the collective dissipation can be rewritten in terms of the LSWT operators as

$$L \simeq \sqrt{2s}\,(a^\dagger + b)\,. \tag{17}$$

Thus, within LSWT, the open-system dynamics is generated by a quadratic Hamiltonian (15) together with a jump operator linear in the bosonic fields (17). As a result, Gaußian states remain Gaußian [CR12, BZ22], and the relevant quantities are the non-zero second moments

$$n_A(t) \equiv \langle a^\dagger a\rangle, \qquad n_B(t) \equiv \langle b^\dagger b\rangle, \qquad m(t) \equiv \langle ab\rangle\,,$$

together with $m^*(t) = \langle a^\dagger b^\dagger\rangle$. The equations of motion follow from the adjoint evolution

$$\frac{d}{dt}\langle O\rangle = -\mathrm{i}\,\langle OH(t)\rangle + \left\langle \mathcal{D}_L^\dagger[O]\right\rangle,$$

which yields the closed system

$$\begin{aligned}
\dot n_A &= -\mathrm{i}B(t)\,(m^* - m) + \frac{1}{2}N\,\Gamma(t)\Big(n_A + 1 + \frac{m+m^*}{2}\Big),\\
\dot n_B &= -\mathrm{i}B(t)\,(m^* - m) - \frac{1}{2}N\,\Gamma(t)\Big(n_B + \frac{m+m^*}{2}\Big),\\
\dot m &= -2\mathrm{i}A(t)\,m - \mathrm{i}B(t)\,(1 + n_A + n_B) + \frac{1}{4}N\,\Gamma(t)\,(n_B - n_A - 1),
\end{aligned} \tag{18}$$

which is derived in Appendix B.3, with the remaining equations obtained by complex conjugation. These equations provide a description of the collective dissipative dynamics within LSWT, reducing the open-system evolution to a small set of coupled ordinary differential equations that can be integrated efficiently throughout the ramp.

Finally, the squeezing parameter (12) can be written directly in terms of the second moments evolved above. Using the LSWT expressions (44), one obtains

$$\xi^2_{\mathrm{bos}} = \frac{(N/2)^2}{(N/2 - n_A - n_B)^2}\left[n_A + n_B + 1 + 2\mathrm{Re}(m)\right] \tag{19}$$

The initial AFM vacuum has $n = 0$ and $m = 0$, giving $\xi^2_{\mathrm{bos}} = 1$. Values $\xi^2_{\mathrm{bos}} < 1$ indicate squeezing, which requires the buildup of a negative two-mode correlation $m_{\mathrm{Re}} < 0$ between the two sublattices. The imaginary part m_{Im} does not enter the squeezing parameter directly, but it affects its time evolution through the coupled equations of motion.

4.2 Results and discussion

We now use the differential equations (18) obtained within LSWT to study the preparation of squeezed antiferromagnetic states for larger atom numbers. The system is initialised in the AFM product state, which corresponds to the bosonic vacuum, so that

$n_A(0) = n_B(0) = m(0) = 0$. For each value of system size N, adiabatic parameter ϵ_0 and dissipation strength η, the equations of motion (18) are integrated along the locally optimised ramp (16), and the squeezing is evaluated using Eq. (19).

We first analyse the time evolution of the squeezing introduced in the system for different adiabatic tolerance at a fixed atom number and dissipation parameter. This allows us to see how the collective squeezing $\xi^2_{\rm bos}$ (19) develops during the protocol and how the minimum value of $\xi^2_{\rm bos}$ changes as the system size is increased.

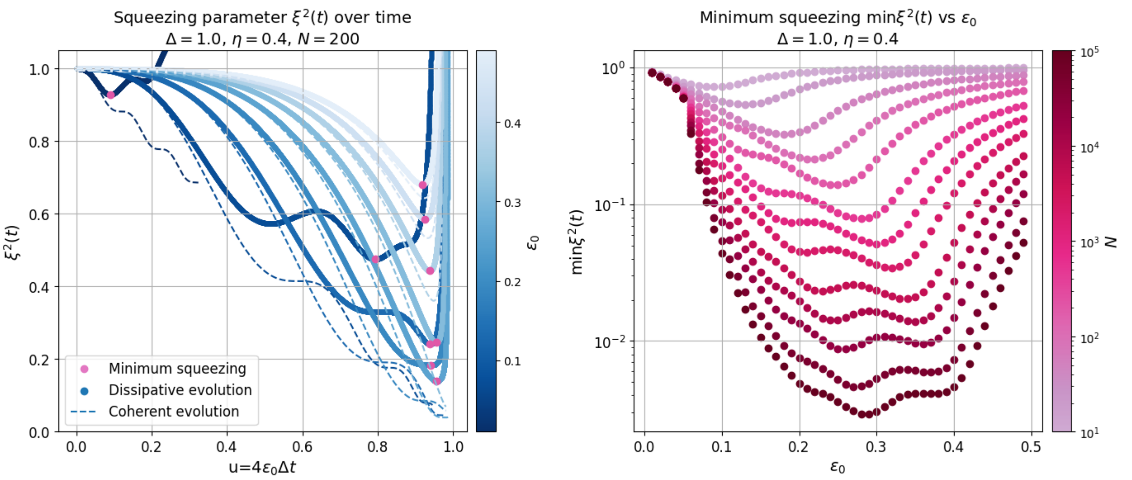

Figure 4: Effect of the adiabaticity on the antiferromagnetic squeezed state for $\Delta = 1.0$ and $\eta = 0.4$. The left panel shows the squeezing parameter (19) for $N = 200$ and different adiabatic parameters ϵ, distinguishable by colour. The dashed lines represent the same trajectories in the coherent scenario ($\eta = 0$). The pink markers indicate the minimum $\xi^2_{\rm bos}$ reached along each trajectory. These values are then plotted in the right panel as a function of ϵ_0 for different atom numbers N.

Figure 4 makes explicit the dependence of the squeezing on the adiabatic parameter and on the stopping time. In the left panel, we can see that $\xi^2_{\rm bos}$ initially decreases from its AFM value $\xi^2_{\rm bos} = 1$, indicating the generation of collective quantum correlations between the two sublattices. However, the system reaches a point where the accumulated dissipation is strong enough to produce large losses and squeezing increases again. This behaviour implies an optimal stopping time where the protocol reaches its maximal efficiency. In the right panel, the protocol has been optimised over time and highlights the best outcome of the protocol for a particular set of parameters (N, ϵ_0) with fixed $\eta = 0.4$. For a fixed atom number N we get back to the error competing mechanism. For small ϵ_0, the ramp is slow and the system spends more time exposed to collective dissipation. For large ϵ_0, the ramp is faster but diabatic errors reduce the amount of squeezing generated. Between these two regimes there is an optimal value of ϵ_0, where the two effects are balanced. As N increases, the minimum value of $\xi^2_{\rm bos}$ decreases, showing that larger systems allow stronger two-mode squeezing.

As in the two atom case, the coherent evolution produces oscillations in the dynamics of the system. These oscillations can be understood from the equation of motion for the pair correlator $m = \langle ab \rangle$. In the absence of collective dissipation, this equation reduces to

$$\dot{m} = -2\mathrm{i}A(t)\, m - \mathrm{i}B(t)\, (1 + n_A + n_B)\,.$$

The term proportional to $B(t)$ generates pair correlations, while the term proportional

to $A(t)$ rotates their complex phase. In the ideal adiabatic limit, $m(t)$ would remain at its instantaneous ground-state value. But for a finite ramp speed, the correlator develops a small deviation from this value. The coherent rotation of this deviation produces oscillations in $\mathrm{Re}(m)$ and, in the squeezing parameter ξ^2_{bos}.
The right panel in Fig. 4 shows that, for each system size, there is an optimal ϵ_0 that generates the maximum squeezing. This fixes the optimal adiabatic tolerance ϵ_0 and provides a single measure of the best squeezing achieved for a given atom number N and a particular dissipation strength η. In Fig. 5, we see the relation between these four magnitudes.

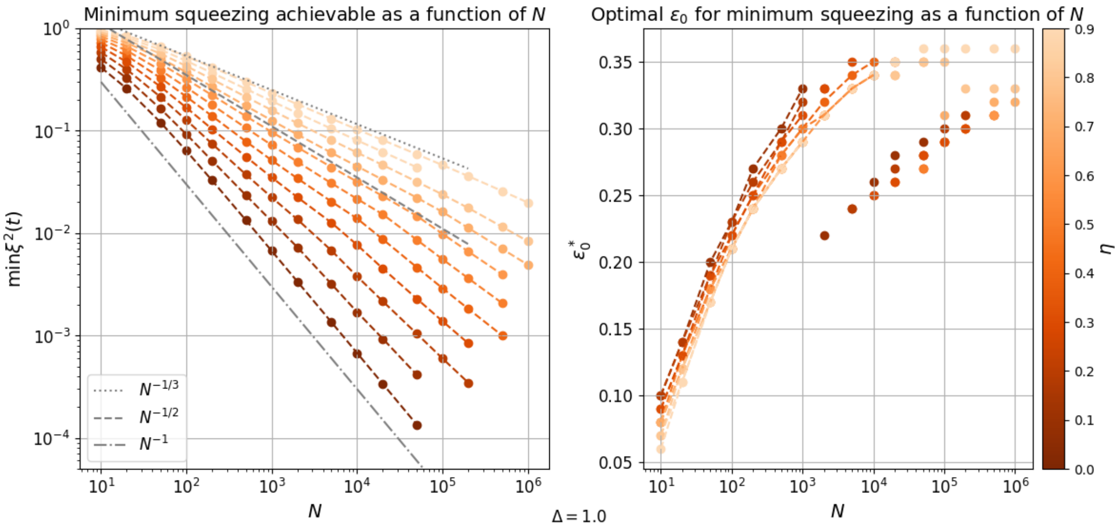

Figure 5: Dependence of the optimised squeezing protocol on the atom number N and dissipation strength η, for $\Delta = 1.0$. Different colours correspond to different values of η. The left panel shows the best achievable squeezing parameter after optimizing over ϵ_0. The dashed grey lines show the reference scalings $N^{-1/3}$, $N^{-1/2}$ and N^{-1}, used as guides to compare the behaviour. The right panel shows the corresponding optimal ramp parameter $\epsilon_0^*(\eta)$, which generally increases with N but has an observable discontinuity.

Figure 5 shows the central qualitative results of the N-atom protocol. The left panel compares the minimum squeezing parameter ξ^2_{min}, optimised over the stopping time and adiabatic parameter, as a function of system size for several values of η. For reference, the power laws $N^{-1/3}$, $N^{-1/2}$, and N^{-1} are also plotted. The right panel shows the corresponding optimal ramp parameter as a function of the system size and the dissipation strength.

The most immediate feature of the left panel is that, for the accessible range of system sizes and η considered, the achievable squeezing improves monotonically with N for every dissipation strength. This means that larger ensembles consistently develop stronger two-mode correlations between the sublattices. However, increasing the collective loss strength shifts the curves upward, reducing the amount of achievable squeezing. For weak collective loss, the numerical curves approach a scaling close to the ideal N^{-1} behaviour. In metrological terms, this corresponds to Heisenberg-limited scaling, where the phase sensitivity improves as $1/N$, rather than the standard quantum limit scaling $1/\sqrt{N}$ obtained with uncorrelated particles [GLM04, PSO+18]. This behaviour is non-trivial, but it can be understood from the collective nature of the loss channel. The cavity does not distinguish the two sublattices separately; it couples to their total spin through the jump operator $L = S^A_- + S^B_-$. During the ramp, the correlations that generate squeezing make the transverse fluctuations of the two sublattices partially cancel in this total spin. As a result, the state becomes less visible to the collective emission channel; in other words, it becomes dark. In the ideal singlet limit, the cancellation is complete and the collective jump operator annihilates the state, so it is completely dark.

For stronger dissipation, the scaling becomes weaker, lying closer to intermediate power laws such as $N^{-1/2}$ or $N^{-1/3}$. This indicates that collective loss limits the quantitative amount of squeezing but does not immediately remove the system-size improvement.

The right panel shows that the value of the ramp parameter ϵ_0^* which optimises the squeezing generally increases with N, meaning that larger systems favour faster (less adiabatic) ramps. As the protocol generates increasingly squeezed collective states, the state can become progressively less bright under the collective emission channel. Consequently, the optimal ramp speed is set by the interplay between coherent squeezing, collective emission, and the stability of the dynamical trajectory. Therefore, the observed drift of $\epsilon_0^\star$ with system size may reflect the fact that larger systems can reach strong squeezing over shorter effective ramp times before dissipative or dynamical instabilities dominate. The right panel also presents a sharp jump that originates from coherent oscillations in the time evolution of $\xi^2(t)$. As shown in Fig. 4, the squeezing dynamics is not strictly monotonic, but it develops oscillations associated with the dynamics of the pair correlations. As a result, each trajectory contains several local minima. As the system size is varied, the identity of the deepest local minimum can change, and the global minimum may switch between different local minima, resulting in a sharp drop in the adiabatic parameter.

Overall, the N-atom results show that collective dissipation reduces the achievable squeezing but does not eliminate the improvement with system size over the range of atom numbers considered. For all values of the collective loss strength studied here, the optimised squeezing parameter decreases monotonically with N within the accessible numerical range. The apparent scaling becomes weaker as the dissipation strength is increased, indicating that collective loss limits the amount of squeezing that can be reached at finite system sizes. However, these results should be interpreted as finite-size effective scalings rather than definitive asymptotic power laws. It remains possible that, at much larger N, the curves cross over to a common asymptotic behaviour. Nevertheless, within the range studied here, the protocol remains effective for generating increasingly correlated states as the number of atoms is increased.

5 Conclusions

In this thesis, we have studied the quasi-adiabatic preparation of squeezed antiferromagnetic states in a collective cavity-QED setting. The motivation was to understand how a classical antiferromagnetic product state can be transformed into an intermediate collective state with reduced total-spin fluctuations, as a first step towards accessing singlet-like many-body physics. The preparation protocol consists of ramping up the cavity-mediated interaction in a finite time, slowly enough to keep the system close to the instantaneous ground state, but without allowing dissipative effects to dominate.

The two-atom problem provided the simplest setting in which the mechanism could be analysed explicitly. In the coherent case, the locally optimised ramp prepares the antisymmetric Bell state with fidelity approaching unity when the ramp is sufficiently slow. Once collective photon loss is included, the best achievable fidelity is reduced, and slower ramps are no longer always optimal. The preparation quality is instead controlled by a competition between diabatic errors, which favour slower evolution, and dissipative losses, which favour shorter protocols. As a result, the best protocol is characterised by an optimal ramp speed, set by ϵ_0, and an optimal stopping time.

For larger atom numbers, linear spin-wave theory allowed us to extend the protocol from the two-atom benchmark to collective many-body ensembles. Within this approximation, the quasi-adiabatic ramp prepares a two-mode squeezed antiferromagnetic state: the total transverse spin fluctuations are reduced while the staggered magnetisation remains finite. This state is not yet a many-body singlet or a quantum spin liquid, but it is the collective intermediate state targeted in the broader preparation strategy. It provides a bridge between the classical AFM product state and the singlet-like regime where additional spatially structured interactions could select more strongly correlated many-body phases.

The many-atom results show that collective dissipation reduces the achievable squeezing but does not remove the improvement with system size. Over the range of atom numbers studied, the optimised squeezing improves monotonically with N for all dissipation strengths considered. In the weak-dissipation regime, the finite-size behaviour is close to the Heisenberg-limited reference, $\xi^2_{\min} \sim N^{-1}$, which is the most favourable scaling expected for this squeezing parameter. Increasing the dissipation weakens this effective scaling, although the squeezing still improves with N over the accessible range. This behaviour reflects the collective nature of the cavity coupling: the correlations generated during the ramp suppress the total transverse spin fluctuations, making the state less bright to the same collective channel that produces photon loss. These scalings should therefore be interpreted as finite-size behaviours rather than definitive asymptotic power laws.

The main conclusion is that the best preparation protocol is not simply the most adiabatic one. It is the protocol that best balances coherent evolution and the accumulation of collective loss. This balance depends on system size and dissipation strength, and it determines both the optimal ramp speed and the optimal stopping time. In this sense, the work identifies the central constraint for using the collective cavity stage as a first step towards correlated antiferromagnetic many-body states. The cavity must generate sufficiently strong collective correlations to suppress total-spin fluctuations, but the preparation must be fast enough to avoid losing those correlations before they can serve as a useful starting point for singlet-like many-body physics.
Several extensions remain open. A natural next step is to benchmark the LSWT predictions against exact collective-spin simulations at intermediate system sizes, in order to determine the range of validity of the bosonic approximation. It would also be useful to optimise ramps directly in the presence of dissipation, rather than using ramps derived from the closed-system adiabatic condition. Another important direction is to include independent local spontaneous emission, which would test how much of the favourable behaviour found here relies on the dissipation being collective. Finally, the squeezed antiferromagnetic states prepared in this work could be used as initial states for the next stage of the broader many-body protocol, where spatially structured interactions are introduced to select specific correlated phases within the singlet-like regime.

Bibliography

[BCK+20] C Broholm, Robert J Cava, SA Kivelson, DG Nocera, MR Norman, and T Senthil. Quantum spin liquids. *Science*, 367(6475):eaay0668, 2020.

[BGGW21] Alexandre Blais, Arne L Grimsmo, Steven M Girvin, and Andreas Wallraff. Circuit quantum electrodynamics. *Reviews of Modern Physics*, 93(2):025005, 2021.

[BZ22] Thomas Barthel and Yikang Zhang. Solving quasi-free and quadratic lindblad master equations for open fermionic and bosonic systems. *Journal of Statistical Mechanics: Theory and Experiment*, 2022(11):113101, 2022.

[Cha24a] Darrick Chang. *Condensed Matter Notes*. 2024.

[Cha24b] Darrick Chang. *Quantum light-matter interfaces: course notes*. 2024.

[CR12] Monique Combescure and Didier Robert. The quadratic hamiltonians. In *Coherent States and Applications in Mathematical Physics*, pages 59–85. Springer, 2012.

[GLM04] Vittorio Giovannetti, Seth Lloyd, and Lorenzo Maccone. Quantum-enhanced measurements: beating the standard quantum limit. *Science*, 306(5700):1330–1336, 2004.

[JC63] Edwin T Jaynes and Frederick W Cummings. Comparison of quantum and semiclassical radiation theories with application to the beam maser. *Proceedings of the IEEE*, 51(1):89–109, 1963.

[LSSV10] Ian D Leroux, Monika H Schleier-Smith, and Vladan Vuletić. Implementation of cavity squeezing of a collective atomic spin. *Physical Review Letters*, 104(7):073602, 2010.

[MNSZ19] Vincenzo Macrı, Franco Nori, Salvatore Savasta, and David Zueco. Optimal spin squeezing in cavity qed based systems. *arXiv preprint arXiv:1902.10377*, 2019.

[MOJ+25] Charlie-Ray Mann, Mark A. Oehlgrien, Błażej Jaworowski, Giuseppe Calajó, Jamir Marino, Kyung S. Choi, and Darrick E. Chang. Squeezing classical antiferromagnets into quantum spin liquids via global cavity fluctuations, 2025.

[MPDR21] Farokh Mivehvar, Francesco Piazza, Tobias Donner, and Helmut Ritsch. Cavity qed with quantum gases: New paradigms in many-body physics. *Advances in Physics*, 70(1):1–153, 2021.

[PSO+18] Luca Pezze, Augusto Smerzi, Markus K Oberthaler, Roman Schmied, and Philipp Treutlein. Quantum metrology with nonclassical states of atomic ensembles. *Reviews of Modern Physics*, 90(3):035005, 2018.

[RDBE13] Helmut Ritsch, Peter Domokos, Ferdinand Brennecke, and Tilman Esslinger. Cold atoms in cavity-generated dynamical optical potentials. *Reviews of Modern Physics*, 85(2):553–601, 2013.

[SB] Lucile Savary and Leon Balents. Quantum spin liquids. *arXiv preprint arXiv:1601.03742*.

[SBY+25] Eric Yilun Song, Diego Barberena, Dylan J Young, Edwin Chaparro, Anjun Chu, Sanaa Agarwal, Zhijing Niu, Jeremy T Young, Ana Maria Rey, and James K Thompson. A dissipation-induced superradiant transition in a strontium cavity-qed system. *Science Advances*, 11(17):eadu5799, 2025.

[SK93] Bruce W Shore and Peter L Knight. The jaynes-cummings model. *Journal of Modern Optics*, 40(7):1195–1238, 1993.

[Ste] Daniel A. Steck. *Quantum and Atom Optics*. Available online at http://steck.us/teaching (revision 0.16.7, 13 March 2026).

[Ste19] Daniel A. Steck. *Quantum Mechanics*. 2019. Available online at https://steck.us/teaching.

[TC68] Michael Tavis and Frederick W Cummings. Exact solution for an n-molecule—radiation-field hamiltonian. *Physical Review*, 170(2):379, 1968.

A The two-atom formalism

In this section, we are going to find the analytical expression for the two-atom coherent Hamiltonian and its eigenenergies, as well as its master equation and the locally optimised ramp for the quasi-adiabatic protocol.

A.1 The two-atom coherent Hamiltonian

Starting from the collective Hamiltonian (4), we will need the expressions for the spin operators. The natural basis for two spins is $\{|\uparrow\uparrow\rangle, |\uparrow\downarrow\rangle, |\downarrow\uparrow\rangle, |\downarrow\downarrow\rangle\}$, but since it conserves the total magnetisation and the initial AFM has $S_z^{\text{tot}} = 0$, the dynamics remains in the two-dimensional subspace $\{|\uparrow\downarrow\rangle, |\downarrow\uparrow\rangle\}$.

For a spin-1/2 particle,

$$S_\alpha = \frac{\sigma_\alpha}{2} \quad \text{and} \quad (S_\alpha)^2 = \frac{\mathbb{1}}{4}\,.$$

Expanding the first term of the Hamiltonian gives

$$\begin{aligned}(S_x^A + S_x^B)^2 + (S_y^A + S_y^B)^2 &= (S_x^A)^2 + (S_y^A)^2 + (S_x^B)^2 + (S_y^B)^2 + 2(S_x^A S_x^B + S_y^A S_y^B) \\ &= \mathbb{1} + S_A^+ S_B^- + S_A^- S_B^+\,,\end{aligned}$$

where we have used the definition $S^\pm = S_x \pm iS_y$. The term $S_A^+ S_B^- + S_A^- S_B^+$ exchanges the two spin configurations in the sector with total magnetization zero. Explicitly, $S_A^- S_B^+ |\uparrow\downarrow\rangle = |\downarrow\uparrow\rangle$ and $S_A^+ S_B^- |\downarrow\uparrow\rangle = |\uparrow\downarrow\rangle$.

On the other hand, the external field term acts as

$$\begin{aligned}(S_z^A - S_z^B)\,|\uparrow\downarrow\rangle &= (S_z^A\,|\uparrow\rangle)\,|\downarrow\rangle - |\uparrow\rangle\,(S_z^B\,|\downarrow\rangle) \\ &= \big(\frac{1}{2}\,|\uparrow\rangle\,\big)\,|\downarrow\rangle - |\uparrow\rangle\,\big(-\frac{1}{2}\,|\downarrow\rangle\,\big) = |\uparrow\downarrow\rangle \\ (S_z^A - S_z^B)\,|\downarrow\uparrow\rangle &= (S_z^A\,|\downarrow\rangle)\,|\uparrow\rangle - |\downarrow\rangle\,(S_z^B\,|\uparrow\rangle) \\ &= \big(-\frac{1}{2}\,|\downarrow\rangle\,\big)\,|\uparrow\rangle - |\downarrow\rangle\,\big(\frac{1}{2}\,|\uparrow\rangle\,\big) = -\,|\downarrow\uparrow\rangle\;.\end{aligned}$$

As a result, the Hamiltonian is

$$H(t) = \begin{pmatrix} \lambda(t) - \Delta & \lambda(t) \\ \lambda(t) & \lambda(t) + \Delta \end{pmatrix}.$$

The term $\lambda(t)\mathbb{1}$ is a global energy shift. It only produces an overall phase in the wavefunction, so it does not affect fidelities or populations. Removing this irrelevant constant and omitting the explicit time dependence, we obtain the effective Hamiltonian

$$H_{\text{eff}}(t) = \begin{pmatrix} -\Delta & \lambda \\ \lambda & \Delta \end{pmatrix}. \tag{20}$$

We proceed with solving the Schrödinger equation

$$H_{\text{eff}}\,|\psi\rangle = E\,|\psi\rangle \tag{21}$$

with $|\psi\rangle = a\,|{\uparrow\downarrow}\rangle + b\,|{\downarrow\uparrow}\rangle$, or in vector form

$$|\psi\rangle = \begin{pmatrix} a \\ b \end{pmatrix} . \tag{22}$$

The eigenvalues are obtained from

$$\det(H_{\text{eff}} - E\mathbb{1}) = \det \begin{pmatrix} -\Delta - E & \lambda \\ \lambda & \Delta - E \end{pmatrix} = 0\,,$$

that gives

$$E^2 - \Delta^2 - \lambda^2 = 0\,.$$

Thus,

$$E_\pm = \pm R \quad \text{where} \quad R = \sqrt{\Delta^2 + \lambda^2}\,. \tag{23}$$

To find the corresponding eigenvectors we solve

$$H_{\text{eff}} \begin{pmatrix} a \\ b \end{pmatrix} = E_\pm \begin{pmatrix} a \\ b \end{pmatrix} \quad \Longleftrightarrow \quad (H_{\text{eff}} - E_\pm\mathbb{1}) \begin{pmatrix} a \\ b \end{pmatrix} = 0\,.$$

From the first row

$$(-E_\pm - \Delta)a \;+\; \lambda b = 0 \Rightarrow \frac{b}{a} = \frac{E_\pm + \Delta}{\lambda}.$$

and imposing normalization

$$|a|^2 + |b|^2 = 1$$

gives

$$a^2 = \frac{\lambda^2}{\lambda^2 + (E_\pm + \Delta)^2} \quad , \quad b^2 = \frac{(E_\pm + \Delta)^2}{\lambda^2 + (E_\pm + \Delta)^2}.$$

Using (23), $\lambda^2 = E_\pm^2 - \Delta^2 = (E_\pm + \Delta)(E_\pm - \Delta)$ and the denominator becomes

$$\begin{aligned} \lambda^2 + (E_\pm + \Delta)^2 &= (E_\pm + \Delta)(E_\pm - \Delta) + (E_\pm + \Delta)^2 \\ &= (E_\pm + \Delta)\big[(E_\pm - \Delta) + (E_\pm + \Delta)\big] \\ &= 2E_\pm(E_\pm + \Delta). \end{aligned}$$

Finally, choosing $a > 0$, we get the instantaneous eigenstates

$$|E_\pm\rangle = \sqrt{\frac{E_\pm - \Delta}{2E_\pm}}|\uparrow\downarrow\rangle \pm \sqrt{\frac{E_\pm + \Delta}{2E_\pm}}|\downarrow\uparrow\rangle. \tag{24}$$

Restoring the explicit time dependence,

$$|E_\pm(t)\rangle = \sqrt{\frac{E_\pm(t) - \Delta}{2E_\pm(t)}}|\uparrow\downarrow\rangle \pm \sqrt{\frac{E_\pm(t) + \Delta}{2E_\pm(t)}}|\downarrow\uparrow\rangle. \tag{25}$$

Defining

$$A(t) = \sqrt{\frac{R(t) + \Delta}{2R(t)}} \quad \text{and} \quad B(t) = \sqrt{\frac{R(t) - \Delta}{2R(t)}}\,, \tag{26}$$

the instantaneous ground and excited states are

$$|g(t)\rangle = A(t)\,|{\uparrow\downarrow}\rangle - B(t)\,|{\downarrow\uparrow}\rangle \tag{27}$$

$$|e(t)\rangle = B(t)\,|{\uparrow\downarrow}\rangle + A(t)\,|{\downarrow\uparrow}\rangle\ . \tag{28}$$

We can rewrite these coefficients in terms of an angle $\theta(t)$ using the definition

$$\cos\theta(t) \equiv \frac{\Delta}{R(t)} \quad , \quad \sin\theta(t) \equiv \frac{\lambda(t)}{R(t)} \quad , \quad \tan\theta(t) = \frac{\lambda(t)}{\Delta}$$

and using the half-angle identities

$$\begin{aligned} A(t) &= \sqrt{\frac{1+\Delta/R(t)}{2}} = \sqrt{\frac{1+\cos\theta(t)}{2}} = \cos\frac{\theta(t)}{2} \\ B(t) &= \sqrt{\frac{1-\Delta/R(t)}{2}} = \sqrt{\frac{1-\cos\theta(t)}{2}} = \sin\frac{\theta(t)}{2} \, . \end{aligned}$$

Therefore, the instantaneous ground and excited states become

$$\begin{aligned} |g(t)\rangle &= \cos\frac{\theta(t)}{2}\,|\uparrow\downarrow\rangle - \sin\frac{\theta(t)}{2}\,|\downarrow\uparrow\rangle \\ |e(t)\rangle &= \sin\frac{\theta(t)}{2}\,|\uparrow\downarrow\rangle + \cos\frac{\theta(t)}{2}\,|\downarrow\uparrow\rangle \, . \end{aligned}$$

A.2 The two-atom protocol

With the analytical expression for the instantaneous eigenstates and eigenenergies, the adiabatic parameter (5) can be calculated analytically.

Since the basis are time independent,

$$|\partial_t g(t)\rangle = \dot{A}(t)\,|\uparrow\downarrow\rangle - \dot{B}(t)\,|\downarrow\uparrow\rangle$$

and

$$\begin{aligned} \langle e(t)\,|\partial_t g(t)\rangle &= B(t)\dot{A}(t) - A(t)\dot{B}(t) \\ &= B(t)\frac{-\Delta\dot{R}(t)}{4A(t)R(t)^2} - A(t)\frac{\Delta\dot{R}(t)}{4B(t)R(t)^2} \\ &= -\frac{\Delta\dot{R}(t)}{4R(t)^2}\Big(\frac{B(t)}{A(t)} + \frac{A(t)}{B(t)}\Big). \end{aligned}$$

Since $A(t)^2 + B(t)^2 = 1$,

$$\begin{aligned} \langle e(t)\,|\partial_t g(t)\rangle &= -\frac{\Delta\dot{R}(t)}{4R(t)^2}\frac{1}{A(t)B(t)} \\ &= -\frac{\Delta\dot{R}(t)}{4R(t)^2}\sqrt{\frac{2R(t)}{R(t)+\Delta}\frac{2R(t)}{R(t)-\Delta}} \\ &= -\frac{\Delta\dot{R}(t)}{2R(t)}\sqrt{\frac{1}{R(t)^2-\Delta^2}} \\ &= -\frac{\Delta\dot{R}(t)}{2R(t)}\sqrt{\frac{1}{\lambda(t)^2}} = -\frac{\Delta\dot{R}(t)}{2R(t)\lambda(t)} \, . \end{aligned}$$

This expression can be rewritten in terms of $\lambda(t), \Delta(t)$ and $\dot{\lambda}(t)$. We have

$$\dot{R}(t) = \frac{\lambda(t)\dot{\lambda}(t)}{R(t)}$$

and thus

$$\langle e(t)\,|\partial_t g(t)\rangle = -\frac{\Delta\dot{\lambda}(t)}{2R(t)^2}\,.$$

On the other hand, using the gap

$$E_+ - E_- = 2R(t) = 2\big[\Delta^2 + \lambda(t)^2\big]^{1/2}$$

we obtain

$$\epsilon(t) = \frac{|\Delta\dot{\lambda}(t)|}{4\big[\Delta^2 + \lambda(t)^2\big]^{3/2}}\,. \tag{29}$$

Imposing the condition $\epsilon(t) = \epsilon_0$ and taking into account that $\dot{\lambda}(t) > 0$, we get the locally optimized coupling speed

$$\dot{\lambda}(t) = \frac{4\epsilon_0}{\Delta}\big[\Delta^2 + \lambda(t)^2\big]^{3/2}\,.$$

Separating variables gives

$$\frac{d\lambda}{\big[D^2 + \lambda^2\big]^{3/2}} = \frac{4\epsilon_0}{D}dt$$

and integrating from 0 to t

$$\begin{aligned}\int_0^{\lambda(t)} \frac{d\lambda'}{\big[\Delta^2 + \lambda'^2\big]^{3/2}} &= \frac{4\epsilon_0}{\Delta}\int_0^t dt' \\ \frac{\lambda(t)}{\Delta^2\sqrt{\Delta^2 + \lambda(t)^2}} &= \frac{4\epsilon_0}{\Delta}t\,.\end{aligned}$$

Solving for $\lambda(t)$,

$$\begin{aligned}\lambda(t) &= 4\epsilon_0\Delta t\sqrt{\Delta^2 + \lambda(t)^2} \\ \lambda(t)^2 &= (4\epsilon_0\Delta t)^2(\Delta^2 + \lambda(t)^2) \\ \lambda(t)^2[1 - (4\epsilon_0\Delta t)^2] &= (4\epsilon_0\Delta^2 t)^2 \\ \lambda(t) &= \frac{4\epsilon_0\Delta^2 t}{\sqrt{1 - (4\epsilon_0\Delta t)^2}}\end{aligned}$$

This ramp naturally gives a maximal duration, determined by the singularity of the denominator

$$t_* = \frac{1}{4\epsilon_0\Delta}\,.$$

In practice, the ramp is stopped at a finite value $\lambda_{\max}$, reducing the duration to

$$T_\lambda = \int_0^{\lambda_{\max}} \frac{d\lambda}{|\dot{\lambda}|} = \frac{\lambda_{\max}}{4\epsilon_0\Delta\sqrt{\Delta^2 + \lambda_{\max}^2}}\,.$$

A.3 The two-atom master equation

We now derive the density-matrix equations for the dissipative $N = 2$ problem. We work in the dynamically accessible product-state basis $\{|\uparrow\downarrow\rangle, |\downarrow\uparrow\rangle, |\downarrow\downarrow\rangle\}$. In this basis, after removing the global energy shift $\lambda(t)\mathbb{1}$, the coherent Hamiltonian is

$$H(t) = \begin{pmatrix} -\Delta & \lambda(t) & 0 \\ \lambda(t) & \Delta & 0 \\ 0 & 0 & 0 \end{pmatrix}\,. \tag{30}$$

The collective lowering jump operator $L = S_-^A + S_-^B$ acts as

$$L|\uparrow\downarrow\rangle = |\downarrow\downarrow\rangle, \qquad L|\downarrow\uparrow\rangle = |\downarrow\downarrow\rangle, \qquad L|\downarrow\downarrow\rangle = 0.$$

Therefore, in this particular basis,

$$L = \begin{pmatrix} 0 & 0 & 0 \\ 0 & 0 & 0 \\ 1 & 1 & 0 \end{pmatrix} \quad \text{and} \quad L^\dagger L = \begin{pmatrix} 1 & 1 & 0 \\ 1 & 1 & 0 \\ 0 & 0 & 0 \end{pmatrix}. \tag{31}$$

The dissipative dynamics is governed by the Lindblad master equation (6).

We now write the most general Hermitian density matrix in this reduced basis as

$$\rho(t) = \begin{pmatrix} p_a(t) & q(t) & u(t) \\ q^*(t) & p_b(t) & v(t) \\ u^*(t) & v^*(t) & p_c(t) \end{pmatrix}. \tag{32}$$

Here, $p_a(t), p_b(t)$ and $p_c(t)$ are populations. Since the density matrix is Hermitian, $\rho^\dagger = \rho$ and its diagonal elements are real. Moreover, since ρ is positive semidefinite, these populations are non-negative and can be interpreted as probabilities. The off-diagonal elements $q(t), u(t)$ and $v(t)$ are coherences and are (in general) complex.

For compactness, in the following derivation we temporarily omit the explicit time dependence of λ, Γ, and the density-matrix elements. First, we compute the coherent contribution $-i[H(t), \rho]$. Multiplying the matrices gives

$$H\rho = \begin{pmatrix} -\Delta p_a + \lambda q^* & -\Delta q + \lambda p_b & -\Delta u + \lambda v \\ \lambda p_a + \Delta q^* & \lambda q + \Delta p_b & \lambda u + \Delta v \\ 0 & 0 & 0 \end{pmatrix},$$

and

$$\rho H = \begin{pmatrix} -\Delta p_a + \lambda q & \lambda p_a + \Delta q & 0 \\ -\Delta q^* + \lambda p_b & \lambda q^* + \Delta p_b & 0 \\ -\Delta u^* + \lambda v^* & \lambda u^* + \Delta v^* & 0 \end{pmatrix}.$$

Therefore, the commutator is

$$[H, \rho] = H\rho - \rho H = \begin{pmatrix} \lambda(q^* - q) & -2\Delta q + \lambda(p_b - p_a) & -\Delta u + \lambda v \\ 2\Delta q^* + \lambda(p_a - p_b) & \lambda(q - q^*) & \lambda u + \Delta v \\ \Delta u^* - \lambda v^* & -\lambda u^* - \Delta v^* & 0 \end{pmatrix},$$

and the coherent part of the master equation is

$$-i[H, \rho] = \begin{pmatrix} -i\lambda(q^* - q) & 2i\Delta q - i\lambda(p_b - p_a) & i\Delta u - i\lambda v \\ -2i\Delta q^* - i\lambda(p_a - p_b) & -i\lambda(q - q^*) & -i\lambda u - i\Delta v \\ -i\Delta u^* + i\lambda v^* & i\lambda u^* + i\Delta v^* & 0 \end{pmatrix}. \tag{33}$$

Next, we compute the dissipative contribution $\mathcal{D}_L[\rho]$. First,

$$L\rho L^\dagger = \begin{pmatrix} 0 & 0 & 0 \\ 0 & 0 & 0 \\ 0 & 0 & p_a + p_b + q + q^* \end{pmatrix}.$$

The anticommutator $\{L^\dagger L, \rho\} = L^\dagger L\rho + \rho L^\dagger L$ gives

$$\{L^\dagger L, \rho\} = \begin{pmatrix} 2p_a + q + q^* & p_a + p_b + 2q & u + v \\ p_a + p_b + 2q^* & 2p_b + q + q^* & u + v \\ u^* + v^* & u^* + v^* & 0 \end{pmatrix}.$$

Therefore, the dissipative part is

$$\mathcal{D}_L[\rho] = \Gamma \begin{pmatrix} -p_a - \mathrm{Re}\, q & -q - \frac{1}{2}(p_a + p_b) & -\frac{1}{2}(u + v) \\ -q^* - \frac{1}{2}(p_a + p_b) & -p_b - \mathrm{Re}\, q & -\frac{1}{2}(u + v) \\ -\frac{1}{2}(u^* + v^*) & -\frac{1}{2}(u^* + v^*) & p_a + p_b + 2\mathrm{Re}\, q \end{pmatrix}. \tag{34}$$

Combining the coherent and dissipative parts, we find the following equations of motion:

$$\begin{aligned} \dot{p}_a &= -2\lambda \mathrm{Im} q - \Gamma\left(p_a + \mathrm{Re}\, q\right), \\ \dot{p}_b &= +2\lambda \mathrm{Im} q - \Gamma\left(p_b + \mathrm{Re}\, q\right), \\ \dot{p}_c &= \Gamma\left(p_a + p_b + 2\mathrm{Re}\, q\right), \\ \dot{q} &= 2i\Delta q - i\lambda(p_b - p_a) - \Gamma q - \frac{\Gamma}{2}(p_a + p_b), \\ \dot{u} &= i\Delta u - i\lambda v - \frac{\Gamma}{2}(u + v), \\ \dot{v} &= -i\Delta v - i\lambda u - \frac{\Gamma}{2}(u + v). \end{aligned} \tag{35}$$

These expressions explicitly show that the coherences u and v form a homogeneous subsystem: they are coupled to each other, but they are not sourced by the populations or by the coherence q. Therefore, if at the beginning of the protocol $u(0) = 0$ and $v(0) = 0$, then they will remain zero at all times $u(t) = 0, v(t) = 0$. The coherence q can be decomposed into its real and imaginary parts, $q = x + iy$. With this decomposition, the complex equation for q can be rewritten as two real equations for x and y. Starting from

$$\dot{x} + i\dot{y} = [2i\Delta - \Gamma][x + iy] - i\lambda[p_b - p_a] - \frac{\Gamma}{2}[p_a + p_b],$$

separating real and imaginary parts gives

$$\begin{aligned} \dot{x} &= -2\Delta y - \Gamma x - \frac{\Gamma}{2}[p_a + p_b], \\ \dot{y} &= 2\Delta x - \lambda[p_b - p_a] - \Gamma y. \end{aligned} \tag{36}$$

Including the time dependence again, the full reduced system can be written as a set of five real ordinary differential equations:

$$\dot{p}_a(t) = -2\lambda(t)y(t) - \Gamma(t)\left[p_a(t) + x(t)\right], \tag{37}$$

$$\dot{p}_b(t) = 2\lambda(t)y(t) - \Gamma(t)\left[p_b(t) + x(t)\right], \tag{38}$$

$$\dot{p}_c(t) = \Gamma(t)\left[p_a(t) + p_b(t) + 2x(t)\right], \tag{39}$$

$$\dot{x}(t) = -2\Delta y(t) - \Gamma(t)x(t) - \frac{\Gamma(t)}{2}\left[p_a(t) + p_b(t)\right], \tag{40}$$

$$\dot{y}(t) = 2\Delta x(t) - \lambda(t)\left[p_b(t) - p_a(t)\right] - \Gamma(t)y(t). \tag{41}$$

These expressions clearly separate the coherent dynamics from the collective dynamics governed by $\lambda(t)$ and $\Gamma(t)$ respectively.

B The N-atom formalism

In this section, we are going to find the analytical expression for the N-atom coherent Hamiltonian and its eigenenergies, as well as the quasi-adiabatic protocol and the equations of motion when the collective dissipation is taken into account.

B.1 The N-atom coherent Hamiltonian

Starting from the collective Hamiltonian (4), we want to find an expression for the Hamiltonian in the LSWT approximation. We first rewrite the transverse spin components in terms of ladder operators,

$$\left(S_x^A + S_x^B\right)^2 + \left(S_y^A + S_y^B\right)^2 = \frac{1}{2}\left(S_+S_- + S_-S_+\right),$$

where $S_+ = S_+^A + S_+^B$ and $S_- = S_-^A + S_-^B$. We now expand the spin ladder operators using the Holstein–Primakoff transformation (13) and truncate them to leading order

$$S_+^A \simeq \sqrt{2s}\, a, \qquad S_-^A \simeq \sqrt{2s}\, a^\dagger,$$
$$S_+^B \simeq \sqrt{2s}\, b^\dagger, \qquad S_-^B \simeq \sqrt{2s}\, b.$$

Therefore,

$$S_+ \simeq \sqrt{2s}\left(a + b^\dagger\right), \qquad S_- \simeq \sqrt{2s}\left(a^\dagger + b\right).$$

Substituting these expressions into the transverse part of the Hamiltonian gives

$$\begin{aligned}\left(S_x^A + S_x^B\right)^2 + \left(S_y^A + S_y^B\right)^2 &\simeq \frac{1}{2}(\sqrt{2s})^2\left[\left(a + b^\dagger\right)\left(a^\dagger + b\right) + \left(a^\dagger + b\right)\left(a + b^\dagger\right)\right] \\ &= 2s\left(a^\dagger a + b^\dagger b + ab + a^\dagger b^\dagger + 1\right),\end{aligned} \tag{42}$$

where we have used the commutation relations

$$[a, a^\dagger] = 1, \quad [b, b^\dagger] = 1, \quad [a, b] = [a^\dagger, b^\dagger] = 0.$$

The longitudinal field term becomes

$$\begin{aligned}-\Delta\left(S_z^A - S_z^B\right) &= -\Delta\left[\left(s - a^\dagger a\right) - \left(b^\dagger b - s\right)\right] \\ &= -2s\Delta + \Delta\left(a^\dagger a + b^\dagger b\right).\end{aligned} \tag{43}$$

Keeping only terms up to quadratic order in the bosonic operators, the Hamiltonian becomes

$$H_{\mathrm{LSWT}}(t) = E_0(t) + [\Delta + 2s\lambda(t)]\left(a^\dagger a + b^\dagger b\right) + 2s\lambda(t)\left(ab + a^\dagger b^\dagger\right),$$

where $E_0(t) = 2s\lambda(t) - 2s\Delta$ is an irrelevant time-dependent constant. Since each sublattice contains $N/2$ spins, its collective spin length is $s = N/4$ and the LSWT Hamiltonian can be written as

$$H_{\mathrm{LSWT}}(t) = E_0(t) + A(t)\left(a^\dagger a + b^\dagger b\right) + B(t)\left(ab + a^\dagger b^\dagger\right), \tag{44}$$

with

$$A(t) = \Delta + \frac{N\lambda(t)}{2}, \qquad B(t) = \frac{N\lambda(t)}{2}. \tag{45}$$

In this form, the Hamiltonian is quadratic in the bosonic operators and can be diagonalized exactly by the Bogoliubov transformation

$$\alpha(t) = \cosh\theta(t)\, a + \sinh\theta(t)\, b^\dagger, \qquad a = \cosh\theta(t)\,\alpha - \sinh\theta(t)\,\beta^\dagger,$$
$$\beta(t) = \cosh\theta(t)\, b + \sinh\theta(t)\, a^\dagger, \qquad b = \cosh\theta(t)\,\beta - \sinh\theta(t)\,\alpha^\dagger.$$

Using the transformations above in the Hamiltonian (44) leads to

$$\begin{aligned} H_{\mathrm{LSWT}}(t) = E_\theta(t) &+ A(t)\big[\cosh 2\theta(t)\,(\alpha^\dagger\alpha + \beta^\dagger\beta) - \sinh 2\theta(t)\,(\alpha^\dagger\beta^\dagger + \alpha\beta)\big] \\ &+ B(t)\big[\cosh 2\theta(t)\,(\alpha\beta + \alpha^\dagger\beta^\dagger) - \sinh 2\theta(t)\,(\alpha^\dagger\alpha + \beta^\dagger\beta)\big]\,. \end{aligned}$$

The parameter $\theta(t)$ is fixed by requiring that the anomalous terms $\alpha\beta + \alpha^\dagger\beta^\dagger$ vanish, which gives

$$\tanh 2\theta(t) = \frac{B}{A} \quad\Longrightarrow\quad \theta(t) = \frac{1}{4}\ln\left(1 + \frac{N\lambda(t)}{\Delta}\right).$$

With this choice, the coefficient of the remaining diagonal terms gives

$$\begin{aligned} A(t)\cosh 2\theta(t) - B(t)\sinh 2\theta(t) &= A(t)\cosh 2\theta(t) - B(t)\frac{B(t)}{A(t)}\cosh 2\theta(t) \\ &= \frac{A(t)^2 - B(t)^2}{A(t)}\cosh 2\theta(t) \\ &= \frac{A(t)^2 - B(t)^2}{A(t)}\frac{1}{\sqrt{1 - \tanh^2 2\theta(t)}} \\ &= \frac{A(t)^2 - B(t)^2}{A(t)}\frac{A(t)}{\sqrt{A(t)^2 - B(t)^2}} \\ &= \sqrt{A(t)^2 - B(t)^2}\,, \end{aligned}$$

where we have used that $\cosh(x) = 1/\sqrt{1 - \tanh^2 x}$. In conclusion, the LSWT Hamiltonian takes the diagonal form

$$H(t) = E_\theta(t) + \omega(t)(\alpha^\dagger\alpha + \beta^\dagger\beta), \tag{46}$$

where $E_\theta(t)$ is the ground-state energy and the Bogoliubov excitation frequency is

$$\omega(t) = \sqrt{\Delta(\Delta + N\lambda(t))}\,. \tag{47}$$

The corresponding instantaneous ground state $|\theta(t)\rangle$ is the Bogoliubov vacuum $\alpha(t)\,|\theta(t)\rangle = \beta(t)\,|\theta(t)\rangle = 0$, which has energy $E_{0,0}(t) = E_\theta(t)$. The lowest excited state in the $S_z = 0$ sector is the pair excitation $|1, 1(t)\rangle \equiv \alpha^\dagger\beta^\dagger\,|\theta(t)\rangle$, which has energy $E_{1,1}(t) = E_\theta(t) + 2\omega(t)$.

B.2 The N-atom protocol

Now we will calculate analytically the adiabatic parameter (5) in order to find the locally optimised ramp for $\lambda(t)$.

The time dependence enters only through the single parameter $\theta(t)$, and thus differentiating gives

$$\partial_t\,|\theta(t)\rangle = \dot\theta(t)\,\alpha^\dagger\beta^\dagger\,|\theta(t)\rangle\,,$$

up to an overall phase convention and

$$\langle 1, 1(t)|\,\partial_t\theta(t)\rangle = \left(\alpha^\dagger\beta^\dagger\,\langle\theta(t)|\,\right)\left(\dot\theta(t)\,\alpha^\dagger\beta^\dagger\,|\theta(t)\rangle\,\right) = \dot\theta(t)\,.$$

So the adiabatic parameter reduces to

$$\epsilon(t) \equiv \left| \frac{\langle 1,1(t)|\, \partial_t \theta(t)\rangle}{E_{1,1}(t) - E_{0,0}(t)} \right| = \frac{|\dot{\theta}(t)|}{2\omega(t)} = \frac{N|\dot{\lambda}(t)|}{8\Delta^2 \left(1 + \frac{N\lambda(t)}{\Delta}\right)^{3/2}},$$

which is controlled by the ratio of the squeezing rate $\dot{\theta}(t)$ to the pair gap $2\omega(t)$. Imposing $\epsilon(t) = \epsilon_0$ and considering $\dot{\lambda} \geq 0$ gives the locally optimised coupling speed

$$\dot{\lambda}(t) = \frac{8\epsilon_0 \Delta^2}{N} \left(1 + \frac{N\lambda(t)}{\Delta}\right)^{3/2}.$$

Separating variables gives

$$\frac{d\lambda}{\left(1 + \frac{N\lambda}{\Delta}\right)^{3/2}} = \frac{8\epsilon_0 \Delta^2}{N} dt$$

and integrating from 0 to t

$$\int_0^{\lambda(t)} \frac{d\lambda'}{\left(1 + \frac{N\lambda'}{\Delta}\right)^{3/2}} = \int_0^t \frac{8\epsilon_0 \Delta^2}{N} dt'$$

$$\frac{2}{N/\Delta}\left[1 - \left(1 + \frac{N\lambda(t)}{\Delta}\right)^{-1/2}\right] = \frac{8\epsilon_0 \Delta^2}{N} t\,.$$

Solving for $\lambda(t)$,

$$\begin{aligned}
1 - \left(1 + \frac{N\lambda(t)}{\Delta}\right)^{-1/2} &= 4\epsilon_0 \Delta t \\
\left(1 + \frac{N\lambda(t)}{\Delta}\right)^{-1/2} &= 1 - 4\epsilon_0 \Delta t \\
1 + \frac{N\lambda(t)}{\Delta} &= (1 - 4\epsilon_0 \Delta t)^{-2} \\
\frac{N\lambda(t)}{\Delta} &= (1 - 4\epsilon_0 \Delta t)^{-2} - 1 \\
\lambda(t) &= \frac{\Delta}{N}\left[(1 - 4\epsilon_0 \Delta t)^{-2} - 1\right]
\end{aligned}$$

This ramp naturally gives a maximal duration, determined by the singularity

$$t_* = \frac{1}{4\epsilon_0 \Delta}.$$

This is in agreement with the two-atom case. If the ramp is stopped at a finite value $\lambda_{\max}$, the time accumulated along the trajectory would reduce to

$$T_\lambda = \int_0^{\lambda_{\max}} \frac{d\lambda}{|\dot{\lambda}|} = \frac{1}{4\epsilon_0 \Delta}\left[1 - \left(1 + \frac{N\lambda_{\max}}{\Delta}\right)^{-1/2}\right]. \tag{48}$$

This locally optimised ramp adapts the instantaneous speed to the local adiabatic condition. As λ grows and becomes comparable to Δ/N, the excitation gap increases and the protocol can accelerate significantly while maintaining the same adiabatic error.

B.3 The N-atom system equations

We now derive the equations of motion for the relevant second moments in the presence of collective dissipation. The expectation value of any operator O evolves according to the Heisenberg equation

$$\frac{d}{dt}\langle O\rangle = -\mathrm{i}\langle[O, H(t)]\rangle + \langle\mathcal{D}_L^\dagger[O]\rangle.$$

The dissipative contribution is generated by the Lindblad dissipator

$$\mathcal{D}_L[\rho] = \Gamma(t)\left(L\rho L^\dagger - \frac{1}{2}\{L^\dagger L, \rho\}\right),$$

where the collective jump operator $L = S_-^A + S_-^B$ can be rewritten in terms of the bosonic ladder

$$L \simeq \sqrt{2s}\,(a^\dagger + b)\,. \tag{49}$$

The corresponding adjoint dissipator acting on observables is

$$\mathcal{D}_L^\dagger[O] = \Gamma(t)\Big(L^\dagger O L - \frac{1}{2}\{L^\dagger L, O\}\Big) = \frac{1}{2}\Gamma(t)\Big(L^\dagger[O, L] + [L^\dagger, O]L\Big). \tag{50}$$

Because the Hamiltonian (46) is quadratic and the jump operator (49) is linear in the bosonic fields, the dynamics of the system is described by the second moments

$$\begin{gathered} n_A = \langle a^\dagger a\rangle, \qquad n_B = \langle b^\dagger b\rangle, \qquad m = \langle ab\rangle, \qquad m^* = \langle a^\dagger b^\dagger\rangle, \\ c = \langle a^\dagger b\rangle, \qquad u_A = \langle a^2\rangle, \qquad u_B = \langle b^2\rangle, \\ c^* = \langle ab^\dagger\rangle, \qquad u_A^* = \langle (a^\dagger)^2\rangle, \qquad u_B^* = \langle (b^\dagger)^2\rangle. \end{gathered}$$

We first derive the closed coherent equations, which correspond to the first term of the Heisenberg equation. For the expectation value $\langle a^\dagger a\rangle$,

$$\frac{d}{dt}\langle a^\dagger a\rangle = -\mathrm{i}B(t)\big(-\langle ab\rangle + \langle a^\dagger b^\dagger\rangle\big) \quad\Rightarrow\quad \dot{n}_A = -iB(t)(m^* - m),$$

while the corresponding equation for $\langle b^\dagger b\rangle$ is obtained by exchanging $a \leftrightarrow b$ and lead to the same equation. Similarly, for the mixed expectation value $\langle ab\rangle$ one finds

$$\frac{d}{dt}\langle ab\rangle = -2\mathrm{i}A(t)\langle ab\rangle - \mathrm{i}B(t)\big(\langle a^\dagger a\rangle + \langle b^\dagger b\rangle + 1\big) \quad\Rightarrow\quad \dot{m} = -2iA(t)m - iB(t)(n_A + n_B + 1).$$

We now consider the correlator $c = \langle a^\dagger b\rangle$. Using the above commutators, its coherent time evolution is

$$\frac{d}{dt}\langle a^\dagger b\rangle = -\mathrm{i}A(t)\Big(-\langle a^\dagger b\rangle + \langle a^\dagger b\rangle\Big) - \mathrm{i}B(t)\Big(-\langle b^2\rangle + \langle (a^\dagger)^2\rangle\Big) \quad\Rightarrow\quad \dot{c} = -iB(t)(u_A^* - u_B).$$

Next, we consider the anomalous correlator $u_A = \langle a^2\rangle$. Its coherent time evolution is

$$\frac{d}{dt}\left\langle a^2\right\rangle = -2\mathrm{i}A(t)\left\langle a^2\right\rangle - 2\mathrm{i}B(t)\left\langle ab^\dagger\right\rangle \quad\Rightarrow\quad \dot{u}_A = -2\mathrm{i}A(t)\,u_A - 2\mathrm{i}B(t)\,c^*.$$

By the same calculation, and using the $a \leftrightarrow b$ symmetry of the coherent dynamics, we obtain for $u_B = \langle b^2\rangle$

$$\dot{u}_B = -2\mathrm{i}A(t)\,u_B - 2\mathrm{i}B(t)\,c.$$

Thus, the coherent dynamics closes on the set $\{n_A, n_B, m, c, u_A, u_B\}$ according to

$$\begin{aligned}
\dot{n}_A &= -\mathrm{i}B(t)(m^* - m), \\
\dot{n}_B &= -\mathrm{i}B(t)(m^* - m), \\
\dot{m} &= -2\mathrm{i}A(t)\, m - \mathrm{i}B(t)(n_A + n_B + 1) \\
\dot{c} &= -\mathrm{i}B(t)(u_A^* - u_B), \\
\dot{u}_A &= -2\mathrm{i}A(t)\, u_A - 2\mathrm{i}B(t)\, c^*, \\
\dot{u}_B &= -2\mathrm{i}A(t)\, u_B - 2\mathrm{i}B(t)\, c,
\end{aligned}$$

where the remaining equations follow by complex conjugation. We now turn to the dissipative contribution. Using the form (50), it is sufficient to evaluate the commutators of O with the jump operator

$$L = S_-^A + S_-^B \simeq \sqrt{2s}\,(a^\dagger + b).$$

We begin with the number operators $n_A = \left\langle a^\dagger a \right\rangle$ and $n_B = \left\langle b^\dagger b \right\rangle$. For $a^\dagger a$, the adjoint dissipator gives

$$\mathcal{D}_L^\dagger[a^\dagger a] = s\Gamma(t)\Big((a + b^\dagger)a^\dagger - (-a)(a^\dagger + b)\Big) = s\Gamma(t)\Big(aa^\dagger + b^\dagger a^\dagger + aa^\dagger + ab\Big).$$

For $b^\dagger b$, one analogously finds

$$\mathcal{D}_L^\dagger[b^\dagger b] = s\Gamma(t)\Big((a + b^\dagger)(-b) - b^\dagger(a^\dagger + b)\Big) = -s\Gamma(t)\Big(ab + b^\dagger b + b^\dagger a^\dagger + b^\dagger b\Big).$$

We next consider the second moments $m = \langle ab \rangle$ and $c = \left\langle a^\dagger b \right\rangle$. For ab, we obtain

$$\mathcal{D}_L^\dagger[ab] = s\Gamma(t)\Big((a + b^\dagger)b - a(a^\dagger + b)\Big) = s\Gamma(t)\Big(b^\dagger b - aa^\dagger\Big).$$

For $a^\dagger b$, we find

$$\mathcal{D}_L^\dagger[a^\dagger b] = s\Gamma(t)\Big(0 - (-b + a^\dagger)(a^\dagger + b)\Big) = s\Gamma(t)\Big(b^2 - (a^\dagger)^2\Big).$$

Finally, we evaluate the dissipator for the anomalous moments $u_A = \langle a^2 \rangle$ and $u_B = \langle b^2 \rangle$. For a^2, this gives

$$\mathcal{D}_L^\dagger[a^2] = s\Gamma(t)\Big((a + b^\dagger)2a - 0\Big) = 2s\Gamma(t)\Big(a^2 + ab^\dagger\Big).$$

For b^2, we analogously obtain

$$\mathcal{D}_L^\dagger[b^2] = s\Gamma(t)\Big(0 - 2b(a^\dagger + b)\Big) = -2s\Gamma(t)\Big(a^\dagger b + b^2\Big).$$

Combining the coherent and dissipative contributions, we arrive at the following closed system of coupled differential equations:

$$\begin{aligned}
\dot{n}_A &= -\mathrm{i}B(t)(m^* - m) + \frac{N}{4}\Gamma(t)(2n_A + 2 + m + m^*), \\
\dot{n}_B &= -\mathrm{i}B(t)(m^* - m) - \frac{N}{4}\Gamma(t)(2n_B + m + m^*), \\
\dot{m} &= -2\mathrm{i}A(t)\, m - \mathrm{i}B(t)(n_A + n_B + 1) + \frac{N}{4}\Gamma(t)(n_B - n_A - 1), \\
\dot{c} &= -\mathrm{i}B(t)(u_A^* - u_B) + \frac{N}{4}\Gamma(t)(u_B - u_A^*), \\
\dot{u}_A &= -2\mathrm{i}A(t)\, u_A - 2\mathrm{i}B(t)\, c^* + \frac{N}{2}\Gamma(t)(u_A + c^*), \\
\dot{u}_B &= -2\mathrm{i}A(t)\, u_B - 2\mathrm{i}B(t)\, c - \frac{N}{2}\Gamma(t)(u_B + c),
\end{aligned}$$

where we used $s = N/4$. The equations for m^*, c^*, u_A^*, and u_B^* are obtained by complex conjugation. This system of equations separates into two independent groups. The first group is formed by $\{n_A, n_B, m, m^*\}$. These variables describe the occupations of the two spin-wave modes and the anomalous two-mode correlation $\langle ab\rangle$. Importantly, their equations do not depend on c, u_A, u_B. The second group is formed by $\{c, u_A, u_B\}$, together with their complex conjugates. These variables describe single-particle coherence between the two modes and single-mode anomalous correlations. Since the initial antiferromagnetic product state corresponds to the bosonic vacuum, one has initially $c(0) = u_A(0) = u_B(0) = 0$. The equations above show that with these particular initial conditions, they remain zero throughout the evolution. As a result, for the dynamics considered in this work, it is sufficient to keep only the closed subsystem for $\{n_A, n_B, m, m^*\}$.

To obtain a real system of equations suitable for numerical integration, we separate the real and imaginary parts of the complex correlator m as

$$m = m_{\mathrm{Re}} + \mathrm{i}m_{\mathrm{Im}}, \qquad m^* = m_{\mathrm{Re}} - \mathrm{i}m_{\mathrm{Im}}.$$

From this, it follows that

$$m^* - m = -2\mathrm{i}m_{\mathrm{Im}}, \qquad m + m^* = 2m_{\mathrm{Re}}.$$

Substituting these expressions into the equations for n_A and n_B, we obtain

$$\begin{aligned}
\dot{n}_A &= -2B(t)m_{\mathrm{Im}} + \frac{N}{2}\Gamma(t)\big(n_A + 1 + m_{\mathrm{Re}}\big),\\
\dot{n}_B &= -2B(t)m_{\mathrm{Im}} - \frac{N}{2}\Gamma(t)\big(n_B + m_{\mathrm{Re}}\big).
\end{aligned}$$

Substituting $m = m_{\mathrm{Re}} + \mathrm{i}m_{\mathrm{Im}}$ into the equation for $\dot{m}$, we find

$$\dot{m}_{\mathrm{Re}} + \mathrm{i}\dot{m}_{\mathrm{Im}} = 2A(t)m_{\mathrm{Im}} - 2\mathrm{i}A(t)m_{\mathrm{Re}} - \mathrm{i}B(t)\big(n_A + n_B + 1\big) + \frac{N}{4}\Gamma(t)\big(n_B - n_A - 1\big).$$

Finally, equating real and imaginary parts yields

$$\begin{aligned}
\dot{m}_{\mathrm{Re}} &= 2A(t)m_{\mathrm{Im}} + \frac{N}{4}\Gamma(t)\big(n_B - n_A - 1\big),\\
\dot{m}_{\mathrm{Im}} &= -2A(t)m_{\mathrm{Re}} - B(t)\big(n_A + n_B + 1\big).
\end{aligned}$$

Therefore, the dynamics relevant for the squeezed antiferromagnetic state can be evolved using the real variables $\{n_A, n_B, m_{\mathrm{Re}}, m_{\mathrm{Im}}\}$.